


Fall 2016

# Lab-on-a-chip nucleic-acid analysis towards point-of-care applications

Varun Lingaiah Kopparthy

Follow this and additional works at: <https://digitalcommons.latech.edu/dissertations>

 Part of the [Nanoscience and Nanotechnology Commons](#), and the [Other Biomedical Engineering and Bioengineering Commons](#)

---

**LAB-ON-A-CHIP NUCLEIC-ACID ANALYSIS TOWARDS  
POINT-OF-CARE APPLICATIONS**

by

Varun Lingaiah Kopparthy, B.Tech, M.S.

A Dissertation Presented in Partial Fulfillment  
of the Requirements of the Degree  
Doctor of Philosophy

COLLEGE OF ENGINEERING AND SCIENCE

LOUISIANA TECH UNIVERSITY

November 2016

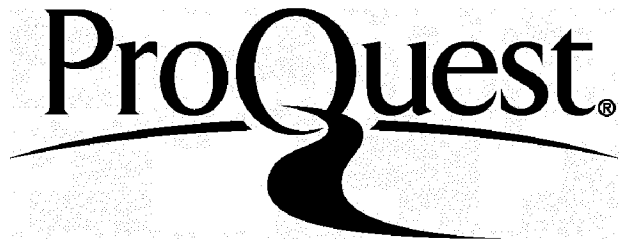
ProQuest Number: 10307852

All rights reserved

INFORMATION TO ALL USERS

The quality of this reproduction is dependent upon the quality of the copy submitted.

In the unlikely event that the author did not send a complete manuscript and there are missing pages, these will be noted. Also, if material had to be removed, a note will indicate the deletion.



ProQuest 10307852

Published by ProQuest LLC(2017). Copyright of the Dissertation is held by the Author.

All rights reserved.

This work is protected against unauthorized copying under Title 17, United States Code.  
Microform Edition © ProQuest LLC.

ProQuest LLC  
789 East Eisenhower Parkway  
P.O. Box 1346  
Ann Arbor, MI 48106-1346

LOUISIANA TECH UNIVERSITY

THE GRADUATE SCHOOL

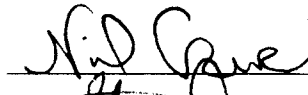
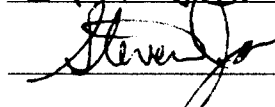
September 29, 2016


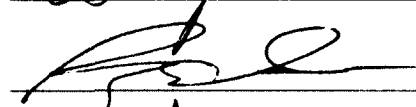
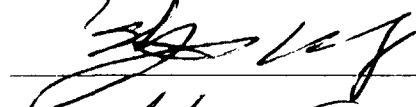
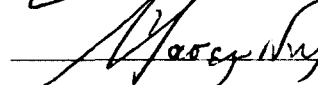
Date

We hereby recommend that the thesis prepared under our supervision  
by Varun Lingaiah Koppaarthi, B.Tech, M.S

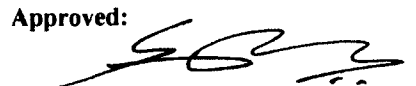
entitled LAB-ON-A-CHIP NUCLEIC-ACID ANALYSIS TOWARDS  
POINT-OF-CARE APPLICATIONS

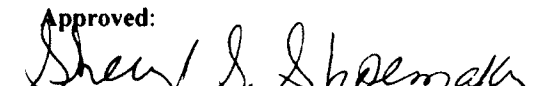
be accepted in partial fulfillment of the requirements for the Degree of  
Doctor of Philosophy in Biomedical Engineering

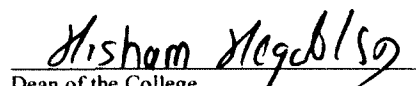
  
\_\_\_\_\_  
Supervisor of Thesis Research  
  
\_\_\_\_\_  
Head of Department  
Biomedical Engineering  
\_\_\_\_\_  
Department

Recommendation concurred in:  
  
\_\_\_\_\_  
  
\_\_\_\_\_  
  
\_\_\_\_\_  
  
\_\_\_\_\_

Advisory Committee

Approved:  
  
\_\_\_\_\_  
Director of Graduate Studies

Approved:  
  
\_\_\_\_\_  
Dean of the Graduate School

  
\_\_\_\_\_  
Dean of the College

## ABSTRACT

Recent infectious disease outbreaks, such as Ebola in 2013, highlight the need for fast and accurate diagnostic tools to combat the global spread of the disease. Detection and identification of the disease-causing viruses and bacteria at the genetic level is required for accurate diagnosis of the disease. Nucleic acid analysis systems have shown promise in identifying diseases such as HIV, anthrax, and Ebola in the past. Conventional nucleic acid analysis systems are still time consuming, and are not suitable for point-of-care applications. Miniaturized nucleic acid systems has shown great promise for rapid analysis, but they have not been commercialized due to several factors such as footprint, complexity, portability, and power consumption.

This dissertation presents the development of technologies and methods for a lab-on-a-chip nucleic acid analysis towards point-of-care applications. An oscillatory-flow PCR methodology in a thermal gradient is developed which provides real-time analysis of nucleic-acid samples. Oscillating flow PCR was performed in the microfluidic device under thermal gradient in 40 minutes. Reverse transcription PCR (RT-PCR) was achieved in the system without an additional heating element for incubation to perform reverse transcription step. A novel method is developed for the simultaneous patterning and bonding of all-glass microfluidic devices in a microwave oven. Glass microfluidic devices were fabricated in less than 4 minutes. Towards an integrated system for the detection of amplified products, a thermal sensing method is studied for the optimization

of the sensor output. Calorimetric sensing method is characterized to identify design considerations and optimal parameters such as placement of the sensor, steady state response, and flow velocity for improved performance. An understanding of these developed technologies and methods will facilitate the development of lab-on-a-chip systems for point-of-care analysis.

## APPROVAL FOR SCHOLARLY DISSEMINATION

The author grants to the Prescott Memorial Library of Louisiana Tech University the right to reproduce, by appropriate methods, upon request, any or all portions of this Dissertation. It is understood that "proper request" consists of the agreement, on the part of the requesting party, that said reproduction is for his personal use and that subsequent reproduction will not occur without written approval of the author of this Dissertation. Further, any portions of the Dissertation used in books, papers, and other works must be appropriately referenced to this Dissertation.

Finally, the author of this Dissertation reserves the right to publish freely, in the literature, at any time, any or all portions of this Dissertation.

Author C. Varun Lingaiah.

Date 11/01/2016

## **DEDICATION**

To

The Lord Almighty;

Mother, Ramadevi Kopparchy;

Father, Prasad Lingaiah Kopparchy;

Sister, Kalambica Kopparchy.



## TABLE OF CONTENTS

ABSTRACT.....	iii
DEDICATION.....	vi
LIST OF TABLES.....	x
LIST OF FIGURES.....	xi
ACKNOWLEDGMENTS.....	xv
CHAPTER 1 INTRODUCTION.....	1
1.1    Polymerase Chain Reaction (PCR).....	3
1.2    Microfluidics.....	7
1.3    Microfluidic PCR.....	10
1.3.1    Stationary Chamber-based PCR.....	11
1.3.2    Continuous-flow PCR.....	12
1.3.3    Oscillating-flow PCR.....	13
1.4    Spatial Gradient Microfluidic Thermal Reactors.....	15
1.5    Quantitative PCR (qPCR) and Melting Detection.....	16
1.6    Spatial PCR and Melting Curve Analysis (MCA).....	17
1.7    Calorimetric Bio-sensing.....	18
1.8    Dissertation Overview.....	21
CHAPTER 2 MICROFLUIDIC THERMAL GRADIENT OSCILLATING-FLOW PCR.....	22
2.1    Introduction.....	22
2.2    State-of-the-Art RT-PCR.....	24

2.3	Materials and Methods.....	25
2.3.1	Microfluidic Device Design and Fabrication.....	25
2.3.2	PCR Reagents .....	26
2.3.3	Microfluidic Chip Loading .....	27
2.3.4	Experimental Setup.....	27
2.4	Results and Discussion .....	29
2.4.1	Thermal Calibration .....	29
2.4.2	Oscillating-flow PCR.....	31
2.4.3	Optimization of RT-PCR for On-chip Detection.....	34
2.4.4	Oscillating-flow RT-PCR .....	39
2.4.4.1	Demonstration of on-chip reverse transcription .....	39
2.4.4.2	On-chip RT-PCR.....	43
2.5	Conclusion .....	44
CHAPTER 3 MICROFAB IN A MICROWAVE OVEN: SIMULTANEOUS PATTERNING AND BONDING OF GLASS MICROFLUIDIC DEVICES.....		45
3.1	Introduction.....	45
3.2	Materials and Methods.....	48
3.2.1	Glass Preparation .....	48
3.2.2	Channel Design.....	49
3.2.3	Assembly and Fusing.....	50
3.3	Experimental Preparation .....	51
3.4	Results and Discussion .....	52
3.4.1	Firing Time .....	52
3.4.2	Microfluidic Channels .....	52
3.5	Conclusion .....	55

CHAPTER 4 MICROSCALE THERMAL BIOSENSOR: CRITICAL DESIGN CONSIDERATIONS AND OPTIMIZATION .....	56
4.1 Introduction.....	56
4.2 Experimental Methods.....	58
4.3 Experimental Setup.....	60
4.4 Experimental Procedure.....	60
4.4.1 Continuous Mixing/Steady State Response .....	61
4.4.2 Bolus Mixing .....	61
4.5 Results and Discussion .....	62
4.5.1 Experimental.....	62
4.5.1.1 Continuous mixing/steady state response.....	62
4.5.1.2 Bolus mixing .....	64
4.6 Conclusion .....	65
CHAPTER 5 CONCLUSIONS .....	66
CHAPTER 6 FUTURE WORK .....	68
6.1 Quantitative Analysis.....	68
6.2 Integration.....	69
APPENDIX A RT-PCR EXPERIMENTAL PROTOCOL .....	70
A.1 Stock Solution Preparation .....	70
A.2 One Step SYBR Prime Script RT-PCR protocol.....	70
A.3 Shuttle PCR.....	73
A.4 Three Step PCR .....	74
BIBILOGRAPHY.....	75

## LIST OF TABLES

<b>Table 3-1:</b> Dependence of firing time on microwave power. ....	50
<b>Table 3-2:</b> Firing time for different COE glass. ....	52
<b>Table A-1:</b> Reagents for one-step RT-PCR. ....	71
<b>Table A-2:</b> Recommended shuttle PCR protocol for Takara kit. ....	73
<b>Table A-3:</b> Recommended three step PCR protocol for Takara kit. ....	74

## LIST OF FIGURES

<b>Figure 1-1:</b> Structure of nucleic acids [5].....	3
<b>Figure 1-2:</b> Schematic of polymerase chain reaction (PCR) thermal cycling mechanism [6].....	5
<b>Figure 1-3:</b> Mechanism of reverse transcription of RNA to cDNA [8].....	6
<b>Figure 1-4:</b> Microfluidic PCR. (a) stationary chamber-based PCR, (b) continuous-flow PCR, and (c) oscillating-flow PCR [20].....	11
<b>Figure 1-5:</b> A steady fluid flow through a steady-state temperature gradient will heat or cool as controlled by the microchannel dimensions and its flow direction within the temperature gradient. ....	16
<b>Figure 1-6:</b> a) During qPCR, the increasing concentration of DNA in the presence of the intercalating dye produces an increased fluorescence. b) As DNA thermally denatures, the intercalating dye is released from the DNA, causing the intensity of the fluorescence to drop. This decrease is proportional to the transition as the double stranded DNA (dsDNA) dissociates into single stranded DNA (ssDNA).....	17
<b>Figure 1-7:</b> (a) Fluorescent image of spatial qPCR. (b) An evaluation of the fluorescence from each cycle reveals the amplification history of the reaction. (c) An evaluate of the fluorescence as a function of temperature within any cycle reveals the sequence-specific melting signature of the PCR product. ....	18
<b>Figure 1-8:</b> Diagram of a thermopile consisting of eight traces of alternating material, placed between two temperatures. If the Seebeck coefficients of the two materials are unequal, a voltage will be transduced in the circuit. Because of the alternating arrangement of junctions, they can be divided into two groups, the measuring junctions (M) and the reference junctions (R). ....	20
<b>Figure 2-1:</b> Schematic of the components of microfluidic device fabrication. (a) shows exploded view of microfluidic device showing glass slides, tape and inlet ports. (b) shows push-pull PCR channel dimensions showing annealing (blue dotted lines), extension (green dotted lines) and denaturation (red dotted lines) regions. ....	26
<b>Figure 2-2:</b> Experimental setup of the thermal gradient oscillating-flow PCR system... ..	29

<b>Figure 2-3:</b> Infrared Images of the thermal gradient on the microfluidic device. (a) no-flow, (b) flow from annealing to denature temperatures, and (c) flow from denature to annealing temperatures. Channel geometry is shown in black dotted line. Arrow in white represents the direction of fluid flow. ....	30
<b>Figure 2-4:</b> Temperature perturbation plots extracted from IR images for (a) no-flow, (b) flow from annealing to denature temperatures, and (c) flow from denature to annealing temperature conditions. ....	31
<b>Figure 2-5:</b> Fluorescence images of melts at various cycles in the PCR. Analysis of the fluorescence in the channel along the dotted green line provides a standard melt curves. ....	32
<b>Figure 2-6:</b> (a) melt curves obtained from analyzing the fluorescence images. The melt curves are separated for better visualization. (b) melt peaks obtained by the first derivative of the standard melt curves. ....	33
<b>Figure 2-7:</b> (a,b,c) are the amplification curve, standard melting curve, and melting peak of the phage DNA PCR using LS-32 system. (d,e,f) are the amplification curve, standard melt curve and the melting peak of the phage DNA PCR using the oscillating-flow system. ....	34
<b>Figure 2-8:</b> Amplification of RNA using individual primers (B2M, GAPDH and GUSB) and melt curve analysis in LS32 system. (a) Amplification curves, b) Standard melt curves, c) Melt peaks. Concentration of RNA used is 40 ng/ $\mu$ l. Reverse transcription time is 5 min and PCR hold times are 20 sec. ....	36
<b>Figure 2-9:</b> Amplification of RNA using multiple primers (B2M and GUSB) and melt curve analysis in LS32 system. (a) Amplification curves, b) Standard melt curves, c) Melt peaks. Concentration of RNA used is 40 ng/ $\mu$ l. Reverse transcription time is 5 min and PCR hold times are 20 sec. ....	37
<b>Figure 2-10:</b> Amplification of RNA using multiple primers (B2M and GAPDH) and melt curve analysis in LS32 system. (a) amplification curve, b) standard melt curve, c) melt peaks. Concentration of RNA used is 40 ng. Reverse transcription time is 1 min and PCR hold times are 0 sec. ....	37
<b>Figure 2-11:</b> Amplification of RNA using multiple primers (B2M and GAPDH) and melt curve analysis in LS32 system. (a) Amplification curves, b) Standard melt curves, c) Melt peaks. Reverse transcription time is 1 min and PCR hold times are 0 sec. ....	38
<b>Figure 2-12:</b> Effect of sample flow in the microfluidic device on $A_{260}/A_{280}$ ratio for RNA quality. ....	40
<b>Figure 2-13:</b> Effect of sample loading in the microfluidic device on RT-PCR efficiency. ....	41

<b>Figure 2-14:</b> Effect of sample interaction with flourinert oil on RT-PCR efficiency.....	42
<b>Figure 2-15:</b> Comparison of on-chip reverse transcription to real-time PCR instrument. Incubation time for reverse transcription is 5 min in both cases. PCR is performed in the real-time instrument after on-chip reverse transcription. ....	42
<b>Figure 2-16:</b> (a) Standard melt curves after RT-PCR in LS32 and in the developed oscillating-flow system. (b) First order derivatives of the standard melts for melting temperature analysis. ....	43
<b>Figure 2-17:</b> (a) High-resolution melt curves after RT-PCR in LS32 and in the developed oscillating-flow system. (b) First order derivatives of the high-resolution melts for melting temperature analysis. ....	44
<b>Figure 3-1:</b> Schematic of the fabrication process.....	48
<b>Figure 3-2:</b> Schematic showing the simultaneous fabrication of glass microchannels and fusing with ceramic impregnated paper. ....	51
<b>Figure 3-3:</b> SEM micrographs of the fabricated microfluidic channels a) cross-section of a straight rectangular channel, b) surface roughness of the channels, c) cross-section of a circular channel, d) surface roughness of the fired ceramic impregnated paper.....	53
<b>Figure 3-4:</b> Microfluidic devices with different flow geometries. a) S-shaped channel, b) straight channel, c) Y-shaped channel, d) smallest feature size channel fabricated using this study. Red and green dyes are used for flow demonstration. ....	55
<b>Figure 4-1:</b> Fabrication of the micro-calorimeter. a) Schematic showing the fabrication of microfluidic device (not drawn to scale). b) Bismuth (Bi)- antimony (Sb) thin film thermopile fabricated on a 50 $\mu\text{m}$ polyimide support. c) Micro-calorimeter: microfluidic device with integrated thermopile.....	59
<b>Figure 4-2:</b> Schematic of the experimental setup. ....	60
<b>Figure 4-3:</b> Fluid flow in the micro-calorimeter showing mixing interface for different flow rate ratios. Dashed white lines represent the walls of the microfluidic device. The dashed red line represents the interface between the fluids driven through inlet 1 and 2. DI water is driven into one inlet, and DI water mixed with green dye is driven into the other inlet. a) Flow rate ratio 1:1 b) flow rate ratio 2:1 and c) flow rate ratio 4:1. ....	61
<b>Figure 4-4:</b> Thermopile output for different flow rate ratios for a total volumetric flow rate of 200 $\mu\text{l}/\text{min}$ . Syringe pumps are programmed to change the flow rate ratios from 1:1, 2:1, and 4:1.....	63
<b>Figure 4-5:</b> Steady state response of micro-calorimeter for different volumetric flow rates a) 100 $\mu\text{l}/\text{min}$ , b) 200 $\mu\text{l}/\text{min}$ and c) 400 $\mu\text{l}/\text{min}$ .....	64

<b>Figure 4-6:</b> Thermopile output for a bolus injection of ethanol sample using an injection valve.....	65
<b>Figure 6-1:</b> Geometry for quantitative analysis.....	69



## ACKNOWLEDGMENTS

This dissertation would not have been possible without the guidance and the help of several individuals who in one way or another contributed and extended their valuable assistance in the preparation and completion of this study.

First and foremost, my utmost gratitude to my committee chairperson, Dr. Niel D. Crews, Director of Institute for Micromanufacturing (IfM) whose sincerity and encouragement I will never forget. I sincerely acknowledge his unselfish and unfailing support.

I am also grateful to my co-advisors, Dr. Steven A. Jones, Dr. Leon Iasemidis, Dr. Shengnian Wang, and Dr. Bryant Hollins, for their technical support and continued interest in this project. Dr. Gergana Nestorova for her valuable suggestions and helping me with the chemistry related to the experiments, and members of Dr. Crews's lab for their support.

I also want to express my deep gratitude to my parents, friends and roommates who constantly supported me throughout this work.

## CHAPTER 1

### INTRODUCTION

Infectious disease outbreaks have shaken the world many times over centuries. Even today, the world lacks powerful scientific tools to combat infectious disease outbreaks. Diagnosis is the first step in treating a disease. The need for a rapid and accurate diagnostic tool has become apparent in the recent Ebola outbreak in December 2013 [1]. Almost a year later, in response to a call by the World Health Organization (WHO) for “rapid, sensitive, safe, and simple Ebola diagnostic tests,” four tests have been approved [2]. These tests include the detection of Ebola-specific RNA, and Ebola virus (EBOV) VP40 antigen. The detection of Ebola-specific RNA relies on the genetic assessment of virus infected patients based on the technology called reverse-transcription polymerase chain reaction (RT-PCR). The tests are slow (takes 2 to 6 hours to process), and usually require some specialized medical personnel to perform the analysis. Also, the tests require an appropriate PCR machine that are oftentimes bulky, limiting them for point-of-care applications. An ideal diagnostic tool must provide fast and sensitive diagnosis, and it must be capable of onsite detection in a limited resource setting [3]. WHO therefore still seeks rapid and diagnostic tools to contain Ebola outbreaks and other future epidemics in general [2].

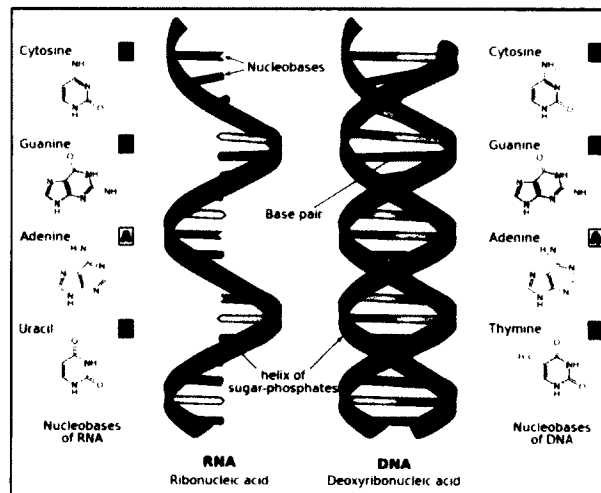
Advances in genetic analysis in recent years have led to the development of nucleic acid based diagnostics. Access to genetic analysis would improve disease

diagnosis, infectious disease treatment and general health. The detection, identification and treatment of diseases have been a major focus of biomedical research. Diagnosis is the first step in treating a disease. Gene expression measurement is an essential tool for molecular biology studies. Several techniques have been developed for quantitative gene expression analysis. With recent advances in microelectromechanical systems (MEMS)-based microfluidic techniques, several research groups have developed nucleic acid analysis. With the development of 'Lab-on-a-chip' systems, there has been a great focus towards developing miniaturized nucleic acid detection systems.

One major hurdle in nucleic acid analysis systems is that the nucleic acid samples collected for analysis from patients or subjects are very low in concentrations. Amplification of the initial sample must be performed to a minimum detection level for existing analysis systems. Polymerase chain reaction (PCR) is widely used for the amplification of the initial nucleic acid sample. Quantitative PCR (qPCR) techniques have become invaluable, high throughput tools to study gene expression. Although microfluidic PCR has been established, many optimizations are still required for successful commercialization of these systems for point-of-care applications. Lab-on-a-chip systems with automated sample handling, amplification and analysis without any post processing steps is desired for fast and accurate diagnosis. This dissertation discloses the optimization of microfluidic PCR for DNA/RNA amplification, reports a new method rapid fabrication microfluidic devices, and investigates thermoelectric bio-sensing method for integrated on-chip detection.

## 1.1 Polymerase Chain Reaction (PCR)

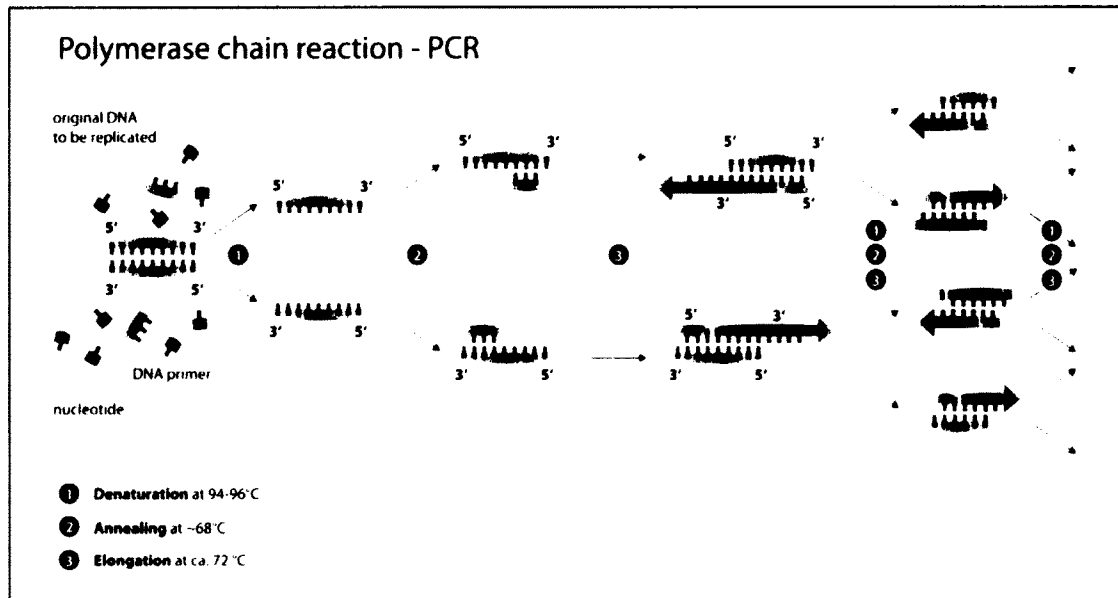
Deoxyribonucleic acid (DNA) carries genetic information used by all living organism for their development and functioning. DNA is composed of nucleotides (dNTPs) that store genetic information. The genetic information is carried out in DNA segments called “genes” [4]. The DNA molecules consist of four different nucleotides that can contain one of the four nitrogen bases – adenine (A), thymine (T), cytosine (C), and guanine (G). Each nucleotide consists of deoxyribose sugar, a phosphate group and a nitrogen base. A particular type of nucleotide on one strand reacts with just a particular type of nucleotide on the other strand. Adenine (A) bonds only to thymine (T), and cytosine (C) bonds only to guanine (G) [4]. Like DNA, ribonucleic acid (RNA) is composed of nucleotides adenine (A), uracil (U), cytosine (C), and guanine (G) (**Figure 1-1**).



**Figure 1-1:** Structure of nucleic acids [5].

Polymerase chain reaction (PCR) is a technique used to amplify DNA. DNA polymerase is an enzyme, which inserts the complementary nucleotide on the single stranded template DNA, thus extending the complementary DNA strand. DNA polymerase is responsible for DNA replication. When a complementary nucleotide is attached to the template, the polymerase enzyme undergoes conformational change that locks the nucleotide within the polymerase and promotes the formation of bonds.

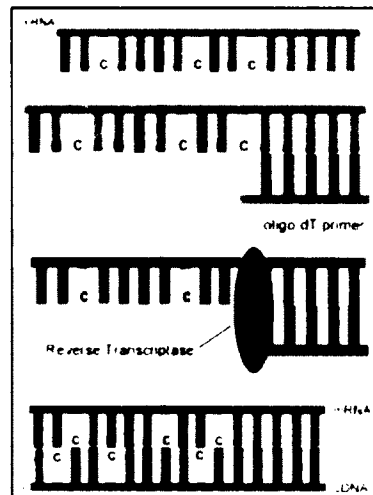
PCR requires cycling between three temperature regions, and reagents such as primers, dNTPs, polymerase enzyme, and buffers for successful amplification of target sequence from a long DNA strand. The three temperature regions enable the following mechanisms in the PCR, 1) denaturation at 94°C to 96°C, 2) annealing at ~68°C, and 3) extension at 72°C. The temperature of the PCR sample is increased to 95°C to reach the denaturation stage, due to the high temperature, the long double stranded DNA separates into single strands. Now the temperature of the PCR sample is decreased to 68°C to reach the annealing stage, the primers (specially designed for target) bind to the 3' (three prime) and 5' (five prime) ends of the target sequence. After this, the temperature of the sample is increased to 72°C to reach to extension stage. At extension, the polymerase enzyme incorporates the complementary nucleotides on both primer ends in forward and reverse, and copies the target sequence (**Figure 1-2**). This thermal cycling process is repeated for about 40 times to obtain multiple copies of the target DNA. Amplification achieved in the PCR cycling is exponential, resulting in 2 copies in the first cycle, 4 copies in the second, and finally  $2^n$  copies in the  $n^{\text{th}}$  cycle.



**Figure 1-2:** Schematic of polymerase chain reaction (PCR) thermal cycling mechanism [6].

Reverse transcription polymerase chain reaction (RT-PCR) is a technique used to amplify segments of RNA and detect RNA expression levels. In RT-PCR, first the RNA is converted to complementary DNA (cDNA) by an enzyme reverse transcriptase. Reverse transcription of RNA to cDNA by transcriptase enzyme requires incubation at 42°C for 5 minutes. Transcriptase transcribes RNA to cDNA by inserting complementary nucleotides in RNA and also replacing uracil (U) with thymine (T) (**Figure 1-3**). The converted cDNA is amplified using standard PCR technique (**Figure 1-2**). RT-PCR is generally carried out in two different protocols, one-step RT-PCR and two-step RT-PCR [7]. In one-step RT-PCR, all the reagents required for the RT-PCR is mixed in a single vial and the process is initiated. Regents such as reverse transcriptase enzyme, RNA primers, dNTPs, DNA polymerase, and DNA primers are all mixed in a single vial, and the RT-PCR is performed. In two-step RT-PCR, first the RNA is mixed with RNA

primers, dNTPs and reverse transcriptase enzyme. Reverse transcriptase enzyme converts RNA to cDNA. The obtained cDNA is added with DNA polymerase enzyme, dNTPs and DNA primers for PCR.



**Figure 1-3:** Mechanism of reverse transcription of RNA to cDNA [8].

These biochemical reactions (PCR/RT-PCR) need strict temperature control in order to perform efficiently. Laboratory instruments for performing these biochemical reactions have been standardized for research use. These instruments are generally bulky and require several hours to achieve results, so they are not suited for point-of-care applications. With the advancement of MEMS, miniaturized PCR systems have been developed for performing lab-on-a-chip. Microfluidics has shown great promise in the lab-on-a-chip field for small sample volumes, efficient heat transfer rates to the sample, and other advantages.

## 1.2 Microfluidics

Microfluidic devices are used in an increasing number of applications in the fields of biochemistry, molecular biology, genomics, microelectronics, and biodefense. These microfluidic systems typically have one or more features with micrometer length scales. Flow in these systems is highly laminar because inertial forces are very low relative to viscous forces. The high degree of laminar flow makes it possible for two fluids to flow parallel without mixing. Microfluidic devices characterized by large surface-to-volume ratios have increased heat and mass transfer efficiencies.

Different techniques were used to create microfluidic devices for biological applications. Techniques such as soft lithography [9], xurography [10], polymer chip development [11], and paper microfluidics [12] has contributed for the simple and rapid fabrication of microfluidic chips for lab-on-chip applications. Recently, researchers have developed shrinky dink microfluidics [10, 11] and PDMS prototyping using a razor blade to fabricate glass microfluidic channels [15], thus eliminating time consuming and complex processes.

Polydimethylsiloxane (PDMS) is widely used in soft lithography for the fabrication of microfluidic devices. PDMS is a soft polymer with inorganic siloxane and organic methyl group attached to silicon [16]. Microfluidic devices with PDMS can be easily cast; the liquid polymer is mixed with the cross linker into a mold with micro-scale features and then bonded it to the glass or plain PDMS sheet. Researchers have exploited this advantage and have used PDMS for fabricating microfluidic devices. PDMS, an elastomer has enabled microfluidic techniques that rely on its inherent flexibility, such as passive valves and integrated peristaltic pumping. However, PDMS does not support



applications that require a rigid substrate, as the PDMS has tendency to collapse. High aspect ratio structures are difficult to fabricate using PDMS and several solvents reacts and swell or dissolve PDMS [17]. The surface of PDMS is hydrophobic and requires passivation for biological applications, high oxygen and water permeability is not desired in some applications, and micro-scale molds are needed initially, which are fabricated using complex lithography procedures. Polymer/thermoplastic and paper microfluidics has shown great promise in the development of lab-on-chip devices for point of care applications. They are flexible and simple to fabricate through a process that does not require complex fabrication techniques. Although these devices are ideal for many biochemical applications, they suffer from limitations such as solvent compatibility and electrode integration [11].

Glass bonding is also used to create microfluidic channels. The surface of the glass is etched according to from the patterns. Patterns are formed using a standard lithography procedure using resist on the glass surface. Then, the glass is placed in hydrofluoric acid (HF) solution to etch the areas in the pattern and another glass is bonded using anodic bonding which requires high temperatures. This technique also requires sophisticated equipment and is expensive. Since the patterns are formed by etching, the surfaces of the channels are not perfectly flat, and might not be suitable when dealing with flow dynamics in the micro channels. Glass microfluidic devices are ideal choice for applications demanding high temperature stability, solvent compatibility, high-pressure flows, and ease of surface passivation [18]. Common methods to fabricate glass microfluidic channels are surface micromachining, buried-channel micromachining, and bulk micromachining [18]. These methods use complex lithography techniques to pattern,

etch, and bond the glass substrates to form microfluidic devices. These processes require harsh chemicals, and technical skill, and they are time consuming. A great deal of optimization is also required to obtain desired specifications.

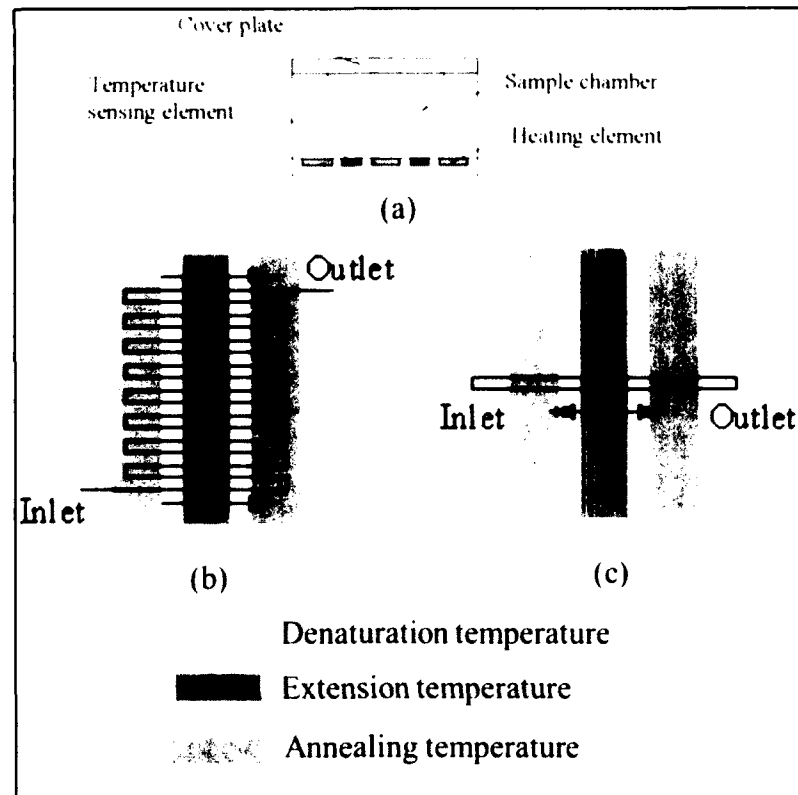
Traditional techniques widely used for fabricating glass microfluidic devices are glass fusion bonding, anodic bonding of glass to silicon, adhesive bonding and assembly, and plasma treatment of PDMS and glass substrate for bonding [18]. In glass fusion bonding, two glass wafers were pressed tightly which enables them to attach each other by Van der Waals forces. The glass stack is then heated at high temperatures ( $>600^{\circ}\text{C}$ ) for long durations, which partially melts the glass at the interface and creates a permanent bond. Anodic bonding involves high temperatures ( $>400^{\circ}\text{C}$ ) and high electric fields (kV) to bond glass to silicon. Sodium ions in the borosilicate glass migrate to the interface and to the silicon under high electric fields and fuse to form a solid chemical bond. Adhesive bonding generally involves use of polymers as adhesives to bond to glass substrates. Polymer materials such as paralyne C, UV cure epoxies, and polyimides.

Applying the adhesive materials as an interfacial layer and heating creates a solid bond between glass substrates. Oxygen or air plasma treatment of PDMS and glass is widely used to fabricate PDMS-glass microdevices. Plasma activates the PDMS and glass surfaces and when in contact creates an irreversible bond. Recently, Kitamori *et al.* developed a technique for room temperature glass-glass bonding using oxygen/tetrafluoromethane ( $\text{CF}_4$ ) reactive ion etching (RIE) plasma treatment [19]. These techniques provide excellent bond strength suitable for high pressure microfluidic applications. Micro-channel fabrication in the substrates in the above techniques still require standard lithography procedures.

Xurography is a simple fabrication technique that uses a cutter to form patterns on a tape. The tape is sandwiched between the glass slides to form micro channels [10]. Double sided adhesive tape is used to form the channels. The glass slides are drilled with holes to introduce fluids into the micro channels. This technique is simple, fast and inexpensive to create microfluidic devices. Xurography uses an adhesive as a sandwich layer between glass or polymer substrates to form microfluidic channels [10]. So the microfluidic devices fabricated using xurography are limited by high pressure flows due to leaking, solvent compatibility-as the acidic or basic solutions will dissolve the adhesive tape, and temperature stability.

### 1.3 Microfluidic PCR

Several research groups have developed miniaturized lab-on-chip PCR devices, which can be broadly categorized into three groups: 1) stationary chamber-based PCR, 2) continuous-flow PCR, and 3) oscillating-flow PCR (**Figure 1-4**).



**Figure 1-4:** Microfluidic PCR. (a) stationary chamber-based PCR, (b) continuous-flow PCR, and (c) oscillating-flow PCR [20].

### 1.3.1 Stationary Chamber-based PCR

In stationary chamber-based PCR [17, 18], standard photolithography is generally used to fabricate a micro well that is filled with the sample. The sample in a micro well is heated and cooled to achieve the three temperature zones (denaturation, annealing, and extension) required for PCR. The small wells can hold very low sample volumes, which is advantageous when the sample availability is low. Limitation of this technology is heating and cooling of the entire micro well chip and sample with thermal mass increases the thermal cycling time [20].

### 1.3.2 Continuous-flow PCR

In continuous-flow PCR, the sample is continuously flown through a microchannel that is placed over three thermal blocks maintained at three temperatures. Continuous-flow PCR in a microfluidic chip was first demonstrated by Kopp et., al in 1998 [23]. This microchip includes serpentine flow channels positioned on heater blocks to produce three temperature zones (denaturation, annealing, and extension). Since this invention, several researchers have developed different techniques to perform continuous-flow PCR [21, 22]. Major limitations of this technique is the thermal cross talk between the temperature regions contributing for inefficient PCR amplification. Crews *et al.*, [26] developed a thermal gradient continuous-flow PCR system by generating a thermal gradient across a glass microfluidic device with serpentine flow channels. When the PCR sample is introduced, the sample undergoes thermocycling by the gradient. This approach eliminates the need for the three thermal regions stringent temperature control. This approach uses a fluorescent intercalating dye which enables spatial analysis of the amplification and melting at the same time without the need for post processing. Since the thermal gradient system depends on the gradient generation on the microfluidic device, generation of a linear gradient and maintaining stable isotherms along the length of the microfluidic device is difficult to achieve. Due to natural convection, the isotherms parabolic in nature indicating the gradient is more linear in the center compared to the edges of the microfluidic device.

Other challenges in continuous-flow PCR related to PCR chemistry also exist such as adsorption of PCR reagents to the microchannel surfaces due to large surface to volume ratio, and cross-contamination of adsorbed reagents [15, 24]. Different surface

coatings were investigated to reduce the adsorption of PCR reagents and the biocompatibility of the micro channels. In addition to the adsorption of PCR reagents, continuous-flow PCR also suffers from the thermal variations on the PCR sample due to the parabolic flow in the micro channels. As the velocity profile is parabolic, the PCR components at the channel surface experience different times for processing compared to the ones in the center.

### 1.3.3 Oscillating-flow PCR

In oscillatory-flow PCR, the sample is shuttled between the three thermal regions for thermocycling [27]. Oscillatory flow PCR devices have obtained increasing attention in the recent years, due to cycle number flexibility, large footprint reduction, and ability to process multiple samples in parallel [28]. On-chip detection of the amplified products has gained major focus as offline detection is usually time-consuming, labor intensive, and prone to cross-contamination during manual sample loading. Oscillating-flow PCR was first demonstrated by Chiou *et al.*, [29] in a 1 mm inner diameter capillary by shuttling PCR sample plug between three thermocycling zones. Capillary-based oscillating-flow PCR has been employed extensively in the research community for real-time identification of human genomic sample [30], simultaneous detection of bacteria such as Salmonella, E-coli, and listeria [31], and multiplex detection of food borne bacterial pathogens [28].

Glass capillaries were widely used for oscillating-flow PCR, in the recent year's materials such as PTFE, PMMA, COC and PDMS were explored. Apart from the capillary-based method, several microfluidic chip configurations were developed to facilitate oscillating-flow PCR. Furutani *et al.* [32] developed a chip with distinct

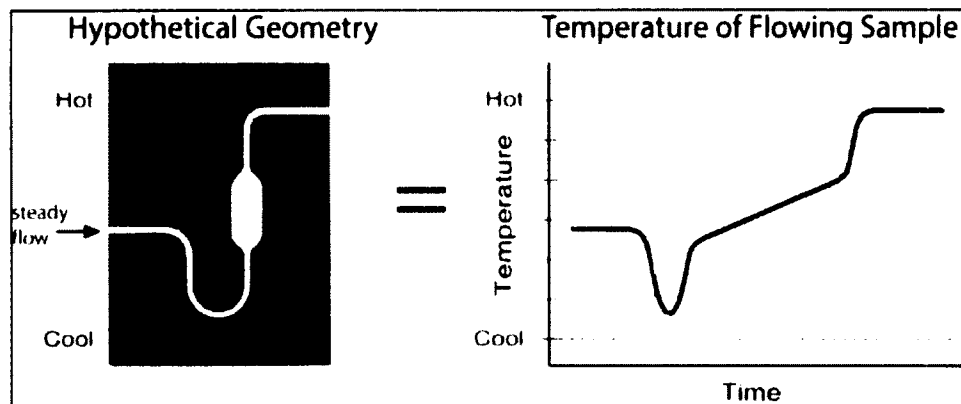
serpentine channels connected for shuttling the flow between denature and annealing temperatures using micro blowers instead of syringe pumps for precise handling of the fluid. Similarly, Brunklas *et al.* [33] developed a microfluidic chip with distinct serpentine channels connected for different thermal regions. The microfluidic chip does not contain a vented channel at ambient pressure. Instead, a closed end channel is used. The sample is pushed used a syringe pump against the closed end channel, and is released for flow in the backward direction. The authors reported an ultrafast PCR using this approach achieving amplification in 6 min. Sciancalepore *et al.* [34] developed a microchannel with integrated heaters for thermal regions. Nested PCR was demonstrated in this device in less than 50 min. Cheng *et al.* [35] developed a radial temperature gradient in a disc type microfluidic device. Early oscillating-flow PCR devices required offline detection of the amplified products such as gel electrophoresis. Although several groups have incorporated online fluorescence detection, amplification efficiency of the sample could only be determined. Quantitative real-time analysis of PCR and melting detection is still not possible in oscillating-flow PCR methodology.

In this dissertation, oscillatory-flow PCR with in a thermal gradient system is proposed. The design of the microfluidic channel and the thermal gradient setup system facilitates the thermocycling via temperature gradient. Intercalating dye-based fluorescence detection enables real-time detection of amplification and melting. This system offers quantitative real-time nucleic acid analysis. As the thermocycling is achieved by thermal gradient, additional temperature blocks are not required for the RT-PCR for the reverse transcription step. Design of the microfluidic device and control of the gradient set temperatures allows for flexibility for both PCR and RT-PCR.

#### 1.4 Spatial Gradient Microfluidic Thermal Reactors

Commercially-available instruments require high power (~500W) and complex feedback control in order to maintain the required temperature cycling within acceptable limits. Niel Crews has developed microfluidic methods that circumvent the typical challenges of creating rapid and high-precision temperature histories. In this method, heating and cooling occurs spatially instead of temporally. Temperature is a function of position so the temperature distribution is passive (naturally occurring) rather than active (modulating power to increase or decrease temperature). In this approach, spatial temperature control (stable or cycling) is achieved by: A) creating a stable temperature gradient across a small glass substrate containing a microfluidic channel, and B) flowing samples through the channel at a constant volumetric flow rate. As aqueous samples flow through the microchannel they are heated and cooled by the channel walls through which they pass. Because of the high surface-to-volume ratio inherent in such microfluidic structures, each sample reaches the temperature of the glass in less than 100 ms [23]. As depicted in **Figure 1-5**, the temperature profile experienced by the sample is simply a function of the channel geometry, the constant flow rate, and the local orientation of the channel with respect to the temperature distribution in the substrate.

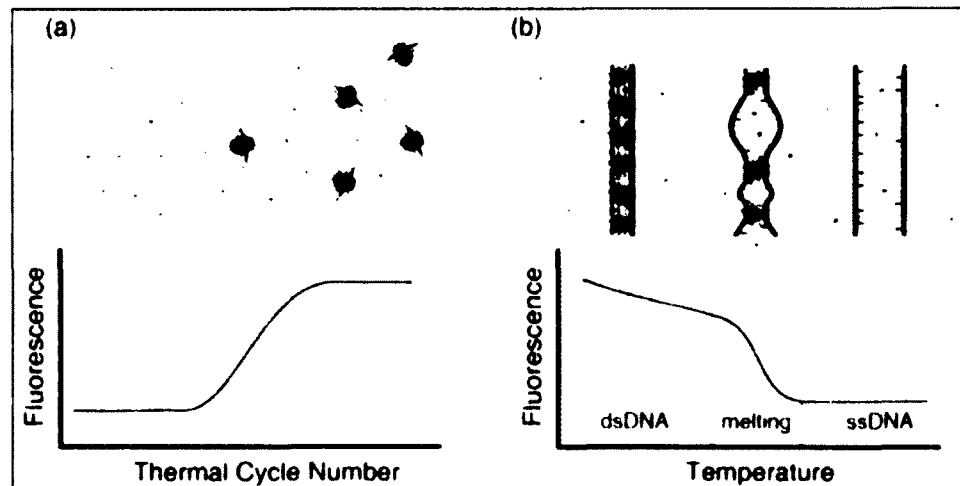




**Figure 1-5:** A steady fluid flow through a steady-state temperature gradient will heat or cool as controlled by the microchannel dimensions and its flow direction within the temperature gradient.

### 1.5 Quantitative PCR (qPCR) and Melting Detection

In order to fluorescently interrogate the amplification of DNA during the PCR, any one of a special family of dyes, called DNA intercalating dyes, are included in the PCR reagent mixture. When in the presence of double-stranded DNA, the dye fluoresces. During amplification, as the quantity of long DNA molecules increases above its detectable threshold, the intensity of the dye increases (**Figure 1-6a**). Additionally, when concentrated DNA and dye is heated above its denaturing temperature, the fluorescence quickly fades (**Figure 2-11b**).

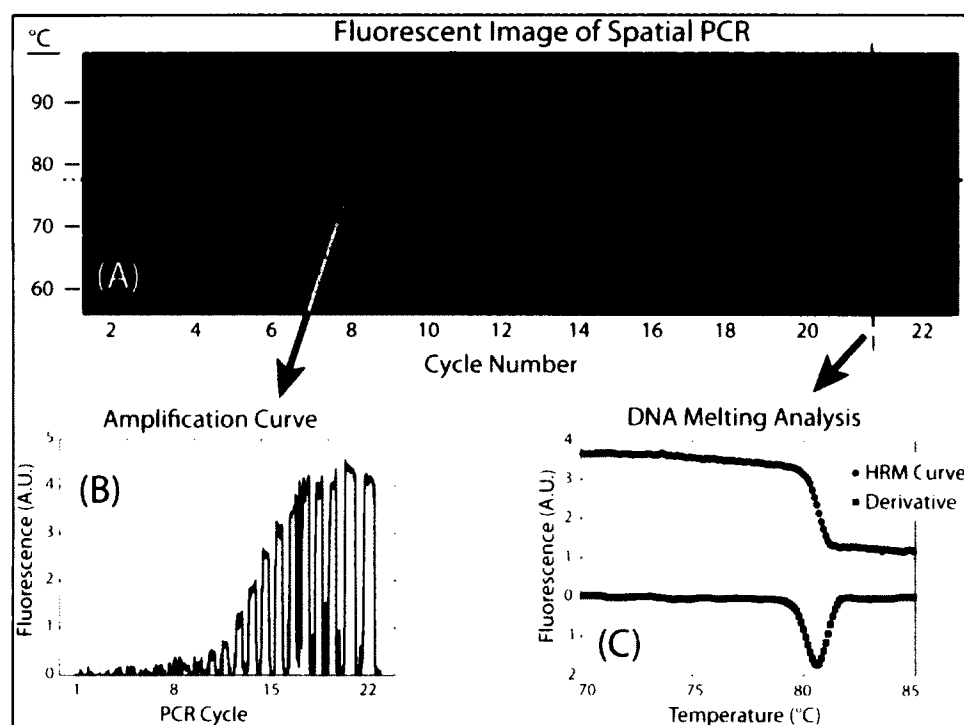


**Figure 1-6:** a) During qPCR, the increasing concentration of DNA in the presence of the intercalating dye produces an increased fluorescence. b) As DNA thermally denatures, the intercalating dye is released from the DNA, causing the intensity of the fluorescence to drop. This decrease is proportional to the transition as the double stranded DNA (dsDNA) dissociates into single stranded DNA (ssDNA).

### 1.6 Spatial PCR and Melting Curve Analysis (MCA)

Conventional qPCR and MCA instrumentation operates on the temporal distribution of temperature, heating and cooling over time. If the microchannel is full of a given sample as it flows, it can be said that the sample is at all temperatures simultaneously. In a situation where the sample contains an intercalating dye and dsDNA, a single photograph captures all the fluorescence data for the temperature span of interest. **Figure 1-7a** shows a spatial qPCR on a microfluidic device [26]. The fluorescence of each cycle can be extracted from the image (**Figure 1-7b**), as can the DNA melting curve at any cycle (**Figure 1-7c**). This technique generates data that is comparable to the HR-1 instrument from BioFire Diagnostics, the gold standard for MCA. However, even a 40-cycle qPCR takes only about 15 minutes in the microfluidic device (at 5 W power consumption), and the data for this spatial analysis was obtained essentially

instantaneously with the click of a camera shutter. The sensitivity of this approach has been highlighted through the demonstration of single nucleotide polymorphism (SNP) genotyping. In a blinded study of 36 clinical DNA samples, point mutations were detected with 100% accuracy [36]. While MCA at the end of PCR has limited value, MCA during the PCR can be used to replicate the amplification curve of each target.



**Figure 1-7:** (a) Fluorescent image of spatial qPCR. (b) An evaluation of the fluorescence from each cycle reveals the amplification history of the reaction. (c) An evaluate of the fluorescence as a function of temperature within any cycle reveals the sequence-specific melting signature of the PCR product.

## 1.7 Calorimetric Bio-sensing

Calorimetric biosensors have been used to detect various analytes such as glucose and urea. The calorimetric approach takes advantage of the universal nature of

heat power production of chemical reactions. These sensors have many advantages over amperometric and optical detection methods such as label-free detection, relatively easy fabrication and less complex detection systems using voltage detectors. Thermopiles are widely used in calorimetric biosensors because they have high common mode thermal noise rejection ratio and can be used with miniaturized devices. Reference junctions of the thermopiles in calorimetric biosensors are controlled either by a constant heat source, heat sink or by vacuum encapsulation. Controlling reference temperature adds complexity to the system and requires additional components. The thermopiles' high common mode rejection of thermal signals enables development of a label-free, highly-sensitive, interferent-free device without need to control reference junction temperature.

A thermopile is a temperature or radiation sensor that is formed by placing multiple thermocouples in a series. The result is a series of wires or traces with alternating material properties. In the presence of a temperature gradient, an electric potential ( $\Delta V$ ) forms in each trace that is a function of the temperature difference ( $\Delta T$ ) between interconnects and the Seebeck coefficient ( $S$ ) of the material itself:

$$\Delta V = S \Delta T \quad \text{Eq. 1-1}$$

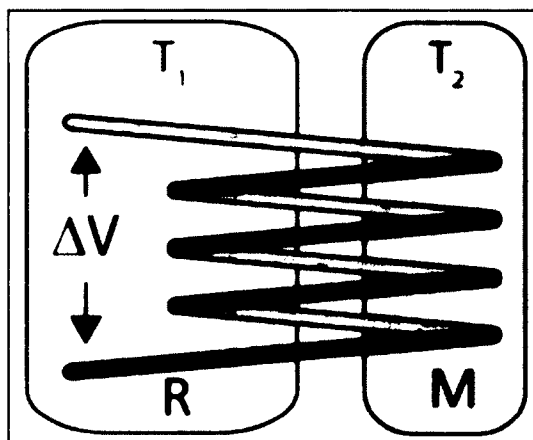
The total voltage transduced in a circuit will be the sum of all these individual voltages:

$$\Delta V = \sum_i S_i (\Delta T)_i \quad \text{Eq. 1-2}$$

When materials with dissimilar Seebeck coefficients are selected, alternating positive and negative temperature differences (**Figure 1-8**) can transduce a cumulative voltage. Common thermopile material pairs include antimony ( $S=48.9 \mu\text{V/K}$ ) with

bismuth ( $S = -73.4 \mu\text{V/K}$ ) [11]. Consider the thermopile of **Figure 1-8**, but with an arbitrary ( $n$ ) number of traces of each material. The cumulative voltage in the circuit would be given by:

$$\Delta V = n(S_A(T_2 - T_1) + S_B(T_1 - T_2)) \quad \text{Eq. 1-3}$$



**Figure 1-8:** Diagram of a thermopile consisting of eight traces of alternating material, placed between two temperatures. If the Seebeck coefficients of the two materials are unequal, a voltage will be transduced in the circuit. Because of the alternating arrangement of junctions, they can be divided into two groups, the measuring junctions (M) and the reference junctions (R).

Since voltage is transduced according to the temperature differential ( $\Delta T$ ) across the thermopile, an isothermal condition ( $T_1 = T_2$ ) would result in no voltage change, regardless of the temperature of the thermopile. Therefore, temperature differences, NOT absolute temperatures, are measured. This characteristic, a type of common mode signal rejection, is the basis of virtually all current and historical implementations of thermopile sensing. Another sensor arrangement that is commonly used to achieve this common

mode filtering used for calorimetry applications is an RTD (resistive thermal detector) placed in a Wheatstone bridge configuration.

## 1.8 Dissertation Overview

Chapter 2 introduces the feasibility of thermal gradient oscillating-flow PCR system. The design and fabrication of simple device is presented that can be used for both DNA and RNA amplification. The system was used to perform RT-PCR by maintaining the microfluidic chip at reverse transcription temperature, without any additional modifications to the chip design. The entirety of Chapter 2 is currently in the preparation for submission to a peer-reviewed journal. Chapter 3 reports a new method for the fabrication of all-glass microfluidic devices using a conventional microwave oven. A simple technique has been developed for simultaneous patterning and bonding of glass microchannels in under 2 minutes to 4 minutes depending the type and thickness of the glass used. This technique is believed to be transformative in the field of microfluidics for rapid fabrication of all-glass microfluidic devices. The entirety of Chapter 3 has been submitted to the peer-reviewed journal *Lab on a Chip*, and is currently under review. Chapter 4 discusses the critical design parameters and optimization of thermoelectric sensor for bio-sensing. Specific emphasis is given to the positioning of the sensor, and understanding the steady state response of the system for maximum output. The results in this study will be useful for integrated on-chip detection of the amplified PCR products using a thermoelectric sensor. The entirety of Chapter 4 is currently in preparation for submission to a peer-reviewed journal. Chapter 5 summarizes the results of this dissertation work, and Chapter 6 discusses the future work towards the lab-on-a-chip integration for point-of-care applications.

## **CHAPTER 2**

### **MICROFLUIDIC THERMAL GRADIENT OSCILLATING-FLOW PCR**

#### **2.1 Introduction**

PCR is a technique used to amplify DNA, which carries genetic information used by all living organism for their development and functioning. It is a powerful diagnostic tool to obtain information about the DNA. Oftentimes, the DNA sample obtained from organisms is very low in concentration, making it difficult to analyze by any detection system. PCR is performed to increase the concentration of the initial DNA. PCR is analogous to an electronic amplifier [23] that amplifies a weak signal to a strong one; in PCR the low concentration (weak) DNA is amplified to a higher concentration (strong). Unlike electronic amplifier, PCR is non-linear, and it amplifying in an exponential fashion. PCR amplification is performed by an enzyme, DNA polymerase, which extends the DNA strands by incorporating the nucleotide bases. This reaction requires three temperature regions for denaturation (95°C), annealing (60°C), and extension (72°C) phases. Conventional PCR is a laboratory technique that is time-consuming and has many limitations for point-of-care applications where the diagnosis needs to be readily available. Substantial recent research has focused on developing miniaturized lab-on-a-chip devices for PCR and analysis.

To address the cross contamination in the continuous-flow PCR, researchers have developed droplet PCR technology with small droplets of PCR sample in a carrier fluid such as oil. In addition to decreasing the cross contamination and PCR inhibition, droplet PCR also has faster thermocycling times as the thermal mass of the sample is low. As the sample volumes are low, the entire sample is subjected to heating and cooling at the same time, unlike continuous-flow PCR. Droplet PCR also facilitates to multiple sample analysis as different samples can be used as droplets in a single flow channel, providing a platform for parallel sample analysis. Also, water-in-oil droplets are stable at temperatures greater than 90°C, which improves thermocycling at higher temperature and decreases the formation of bubbles.

Although droplet PCR has several above mentioned advantages over continuous-flow PCR, the droplets are generally passed through long channels over the temperature regions to achieve PCR. Although adsorption of PCR reagents to the channel walls still exist and loss of PCR components from a small droplet can result in inefficient PCR or PCR inhibition. Effective surface coatings to prevent this adsorption are needed.

To address the effective surface to sample volume ratio issue, maintain isotherms in the thermal gradient PCR, and take advantage of the droplet technology, we propose a new channel geometry and programmed flow to infuse (PUSH) and withdraw (PULL) the sample in the channel. Since the sample is pushed and pulled in a definite channel, the surface to volume ratio is low, thereby reducing the adsorption of PCR components to the channel surface. The PCR sample is filled as a droplet plug with oil on both ends to reduce the cross contamination and diffusional dilution of the sample. As the proposed channel geometry is a single vertical channel, it can be located in the center of the



thermal gradient system where the isotherms are straight and the gradient is approximately linear. This eliminated the need for thermal optimization of the gradient system.

## 2.2 State-of-the-Art RT-PCR

Various groups have attempted the detection of RT-PCR in microfluidic devices involving a post processing step for analysis. Some groups have demonstrated RT-PCR in microfluidic devices and have analyzed the amplified product separately using gel electrophoresis [37], [38] and capillary electrophoresis [39], [40]. Some have demonstrated a two-step approach in a single microfluidic device, first performing reverse transcription step and moving the sample into another chamber for PCR. Obeid *et al.* were the first group to integrate RT-PCR in a single microfluidic device [37]. They developed a single monolithic device that can perform RT-PCR with a cycle selection feature [37]. Later, their research group also integrated a laser induced fluorescence detection of the amplified product by moving the amplified product into a fused silica capillary [41]. Problems with these studies were the need for a constant time ratio of 4:4:9 in the PCR and the need for an additional capillary system for amplified product detection.

Lee *et al.* developed a microfluidic MEMS chip for the RT-PCR and integrated micro heaters and micro pumps in the chip, thus eliminating the need for external heaters and pumps [38]. This system lacks on chip detection of the amplified products, and is complex to fabricate and operate. Toriello *et al.* developed a MEMS chip for RT-PCR and used a laser-induced fluorescence technique integrated it with the capillary electrophoresis detection of RNA [39]. Xing *et al.* developed a compact continuous flow

RT-PCR system that used two heated cylinders with spiral tubes for reverse transcription and PCR reactions [42]. Their system also incorporated inline fluorescent detection of the amplified products.

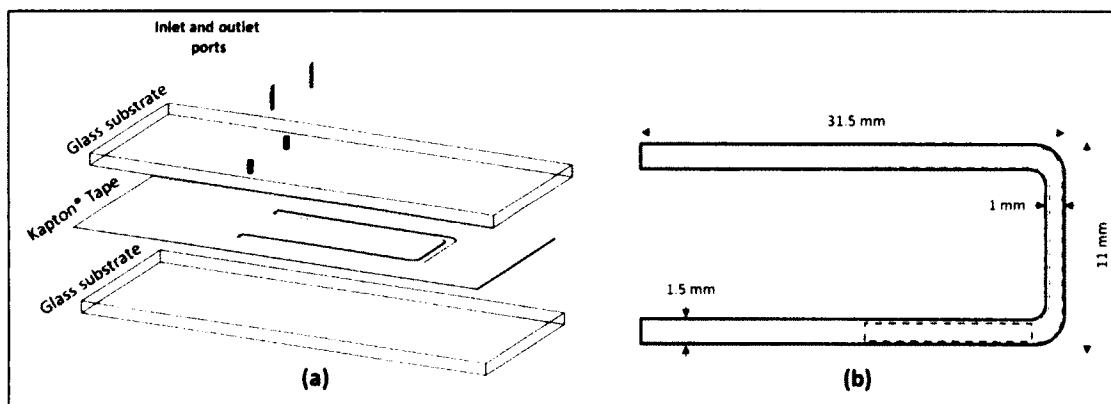
Tamiya *et al.* reported a PDMS microfluidic chip for reverse transcription and a disposable electrical printed (DEP) chip for fast amplification and detection of the amplified products [43]. This method requires additional reagents for electrochemical detection and additional components for voltammetry detection. Recently, Phaneuf *et al.* reported a polymer microfluidic chip with infrared radiation-mediated thermocycling for RT-PCR [44]. This system is complex to fabricate. A rapid on-chip real time RT-PCR system for the fast and accurate analysis of gene expression still needs to be developed.

## 2.3 Materials and Methods

### 2.3.1 Microfluidic Device Design and Fabrication

To fabricate the microfluidic devices, patterned double sided adhesive tape, a poly-dimethyl siloxane (PDMS) sheet, and another double sided adhesive polyimide tape were bonded between two aminosilane-coated glass slides (S4615, Sigma-Aldrich, MO, USA). A cutting plotter (Craft Robo Pro, Graphtech, USA) was used to pattern 100  $\mu\text{m}$  double sided adhesive polyimide tape (PPTDE 1 112, Kaptontape.com, CA, USA) and a 250  $\mu\text{m}$  thick PDMS sheet in the shape of the channel. A fine tip drill bit ((850-010C, NTI, Kahla, Germany) was used to drill holes on a glass slide for fluid inlet and outlet in to the microchannel. The assembly of the microfluidic device with inlets is shown in **Figure 2-1**. Nanports (Upchurch scientific, WA, USA) were attached with superglue over the drilled holes. To clean the glass slide prior to the device fabrication, it was rinsed with 1% solution of detergent (Alconox, NY, USA), followed by distilled water, and dried

with compressed air. PDMS sheet was rinsed with ethanol and dried with compressed air to improve bonding to the double sided polyimide tape. Placing the device in a vice and tightening ensures strong bonding to the glass slides and reduces air bubbles when it is heated for PCR.



**Figure 2-1:** Schematic of the components of microfluidic device fabrication. (a) shows exploded view of microfluidic device showing glass slides, tape and inlet ports. (b) shows push-pull PCR channel dimensions showing annealing (blue dotted lines), extension (green dotted lines) and denaturation (red dotted lines) regions.

### 2.3.2 PCR Reagents

The PCR mixture contained 108 copies/ $\mu\text{l}$  of a viral phage DNA template ( $\phi\text{XI74}$ , New England Biolabs, MA, USA), and 0.5  $\mu\text{M}$  of each of the forward and reverse primers (Integrated DNA Technologies, IA, USA). Primers are 110 bp (F-GGTTCGTCAAGGACTGGTTT, R-TTGAACAGCATCGGACTCAG). A PCR kit (Takara Biosciences, USA) was used to prepare the PCR mixture. A 2X one-step buffer containing deoxynucleotide triphosphate (dNTP), and hot start polymerase enzyme was used from the kit. 2.5 mg/ml bovine serum albumin (BSA) (Sigma-Aldrich MO, USA) was used in the mixture. Intercalating dye, LC Green (LC Green Plus, Idaho Technology,

UT, USA) was used to observe the fluorescence in PCR amplification in both the commercial system (Light scanner system LS-32, Idaho Technology, UT, USA) and the proposed push-pull PCR system. The amplification protocol for the LS-32 consisted of a 1 min initial denaturation at 95 °C, followed by 30 cycles of 95 °C for 1 s, 60 °C for 1 s, and 75 °C for 3s. All temperature ramping on the LS-32 was at a rate of 5 °C/s. At the conclusion of the PCR, a high resolution melting analysis of each amplified sample was performed serially by monitoring the fluorescence during a steady ramp of 0.3 °C/s from 60 °C to 90 °C.

Human RNA (Integrated DNA Technologies, IA, USA), gene specific primers such as B2M, GADH, and GUSB were used for the PCR mixture. Reverse transcriptase enzyme (Takara Biosciences, USA) was used in one-step protocol for RT-PCR. Reverse transcription of RNA to cDNA requires an incubation at 42 °C for 5 min.

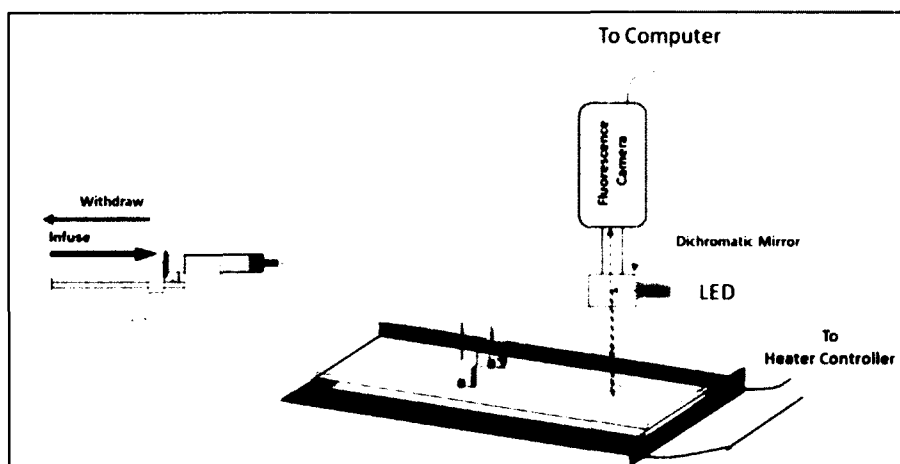
### 2.3.3 Microfluidic Chip Loading

The fabricated microfluidic chip is prepared for testing by flowing 100 µl BSA through the chip at a flow rate of 2 µl/min. BSA binds to the amino saline channel walls and prevents the binding of the intercalating dye, L.C. Green. The chip was rinsed with DI water to remove excess BSA from the chip and is loaded with PCR mixture without any heating for passivating the channel surface. The chip is then emptied and loaded with the PCR sample with fluorinert oil (FC40, Sigma Aldrich MO, USA) making the sample a droplet.

### 2.3.4 Experimental Setup

The thermal gradient system used in this study is previously described as in Pješčić *et al.* [45]. Briefly, a syringe pump (Pump Elite 11, Harvard Apparatus, USA) is

programmed to oscillate the sample at a flow rate of 10  $\mu\text{l}/\text{min}$  between denaturing and annealing temperatures in the microfluidic channel. A schematic of the experimental setup is as shown in the **Figure 2-2**. An in-house fabricated controller and heater system is used to generate thermal gradient across the microfluidic chip. The temperatures on the chip were maintained at 60°C and 90°C for denature and annealing. An infrared camera (A320, FLIR, OR, USA) with a 320×240 pixel array was used to calibrate and validate the temperatures and gradient on chip. A monochrome 1392×1040 (1.4 MP) resolution camera (Pixel Link PL-B957U, ON, Canada) was used to capture images of the chip while the sample is pushed and pulled in the channel. Blue LED lights, 470 nm (Luxeon Star LEDs, USA, MR-B0030-20T) were used as an excitation source for the fluorescence dye. A dichromatic mirror is used to allow excitation and emission in the same line of the camera. Filter sets were used to filter the LED wavelength and the emission wavelength to obtain a sharper quality image. The filter set and dichromatic mirror (Chroma Technology Corporation, USA) were selected based on the spectrum properties: LED filter 425-475 nm (HQ450/50x); camera filter 485-535 nm (HQ510/50nm). Adding a dichromatic mirror 380-750 nm (Q480LP) intensified the LED output on the microfluidic chip, improving the melting analysis image of the channels. Images were recorded for every 45 seconds with an exposure time of 1 second. Recorded images provide the PCR amplification curve and melting analysis simultaneously. Images were analyzed using MATLAB (The MathWorks, MA, USA) to obtain the amplification and melting curves.

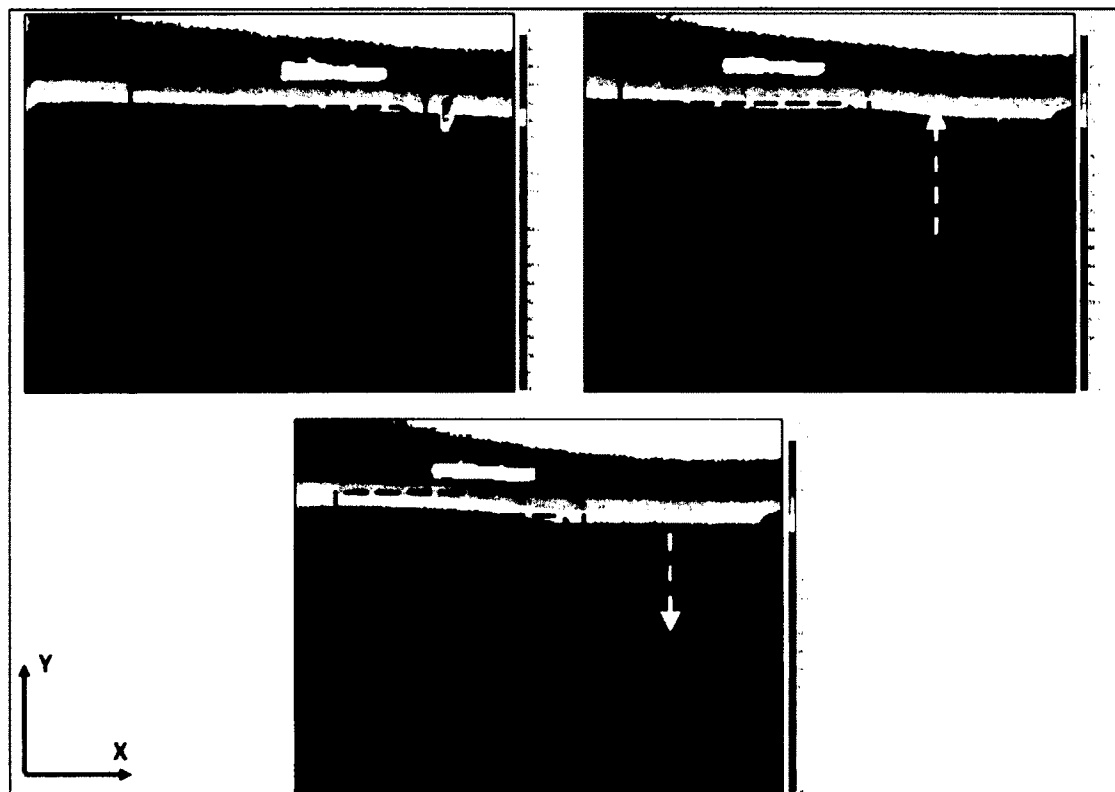


**Figure 2-2:** Experimental setup of the thermal gradient oscillating-flow PCR system.

## 2.4 Results and Discussion

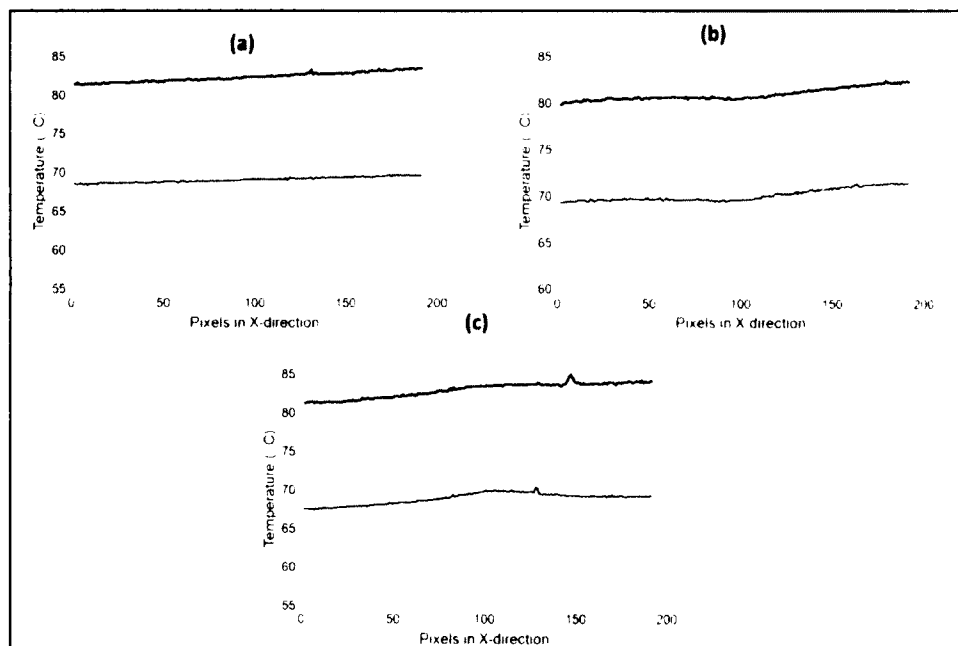
### 2.4.1 Thermal Calibration

The PCR is based on thermocycling of the sample; thermal performance of the device must be characterized to determine the thermal variations. The IR camera is used to characterize the thermal gradient on the chip. Isotherms on the device under no flow and flow conditions are evaluated. The device is loaded with a sample plug (water with 10% BSA) in flourinert oil. The sample is shuttled between the cold and hot temperatures using the syringe pump. Infrared images of the temperature in the microfluidic chip under no flow, and flow conditions are shown in **Figure 2-3**.



**Figure 2-3:** Infrared Images of the thermal gradient on the microfluidic device. (a) no-flow, (b) flow from annealing to denature temperatures, and (c) flow from denature to annealing temperatures. Channel geometry is shown in black dotted line. Arrow in white represents the direction of fluid flow.

Temperatures can be extracted from the pixel values along the X-direction on the IR images. Three different lines in the Y direction are extracted and plotted to see temperature perturbations in all three conditions. Temperature values are plotted for comparison in **Figure 2-4**. The isotherms observed are straight when there is no flow in the microfluidic device. When the sample is shuttled between the annealing and denature temperatures, the flow causes a shift in the isotherms. Temperature perturbations of  $\leq 1.5^{\circ}\text{C}$ , and  $\leq 3^{\circ}\text{C}$  are observed when the sample is moving from annealing to denaturing temperature, and from denaturing to annealing temperature, respectively.

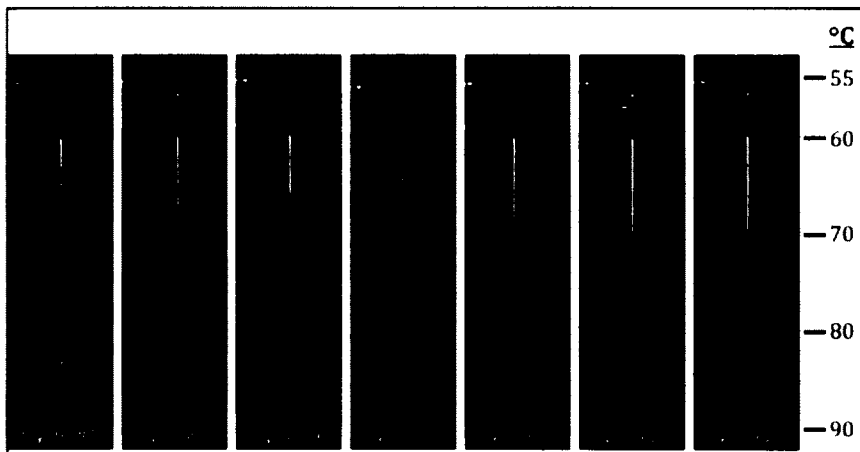


**Figure 2-4:** Temperature perturbation plots extracted from IR images for (a) no-flow, (b) flow from annealing to denature temperatures, and (c) flow from denature to annealing temperature conditions.

#### 2.4.2 Oscillating-flow PCR

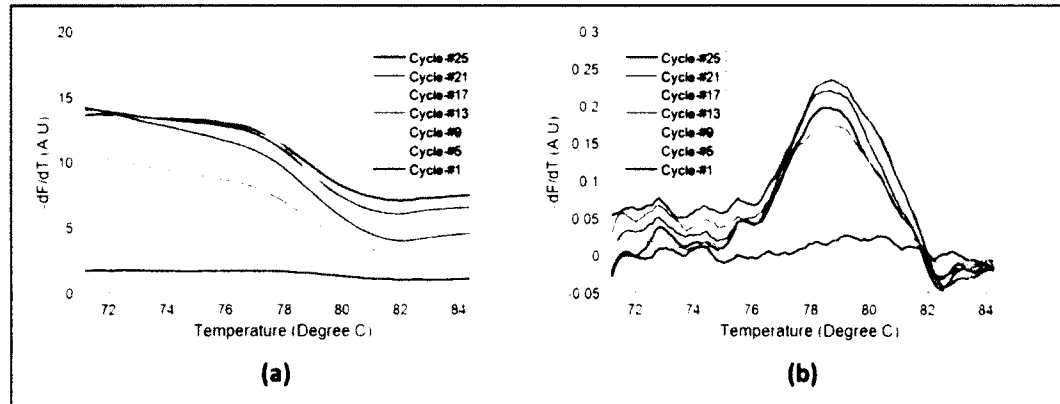
When the PCR sample is oscillated in the microfluidic channel, fluorescence images (**Figure 2-5**) were recorded and analyzed to extract amplification and melt curves. Images recorded during the annealing stages provide the amplification curve, and images at the extension stage; when the sample is flown through the gradient, reveals the melting analysis. Increase in the fluorescence intensity is seen in the recorded images, indicating the amplification process.





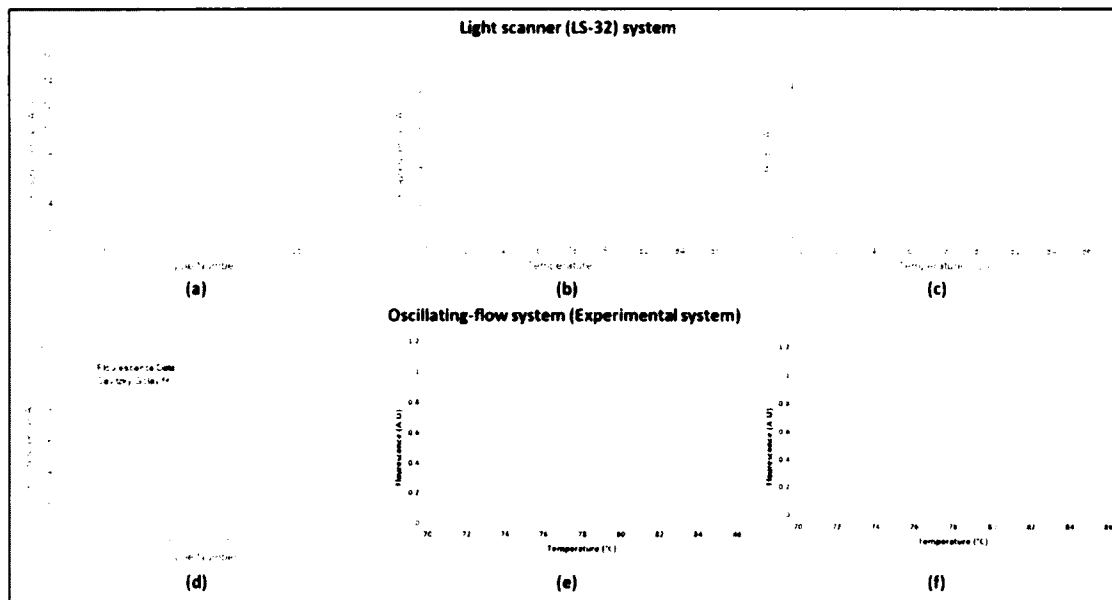
**Figure 2-5:** Fluorescence images of melts at various cycles in the PCR. Analysis of the fluorescence in the channel along the dotted green line provides a standard melt curves.

Extracting the fluorescence data and plotting against cycle number provides amplification curves. Fluorescence values obtained from the dotted green line of **Figure 2-5** are plotted against temperature to provide melt curves. **Figure 2-6** shows the standard melt curves extracted from the obtained fluorescence images. First order derivative of the standard melt produces melt peaks.



**Figure 2-6:** (a) melt curves obtained from analyzing the fluorescence images. The melt curves are separated for better visualization. (b) melt peaks obtained by the first derivative of the standard melt curves.

**Figure 2-7** compares data from the proposed microfluidic oscillating-flow PCR system and the commercially available Light Scanner (LS-32) system. The fluorescent image from the proposed system provides amplification and melting simultaneously. Unlike the LS-32 system, the oscillating-flow system provides the melting analysis at every stage, which is useful when multiple targets are amplified at the same time. Melting analysis provides the cycle at which the individual targets start to amplify.



**Figure 2-7:** (a,b,c) are the amplification curve, standard melting curve, and melting peak of the phage DNA PCR using LS-32 system. (d,e,f) are the amplification curve, standard melt curve and the melting peak of the phage DNA PCR using the oscillating-flow system.

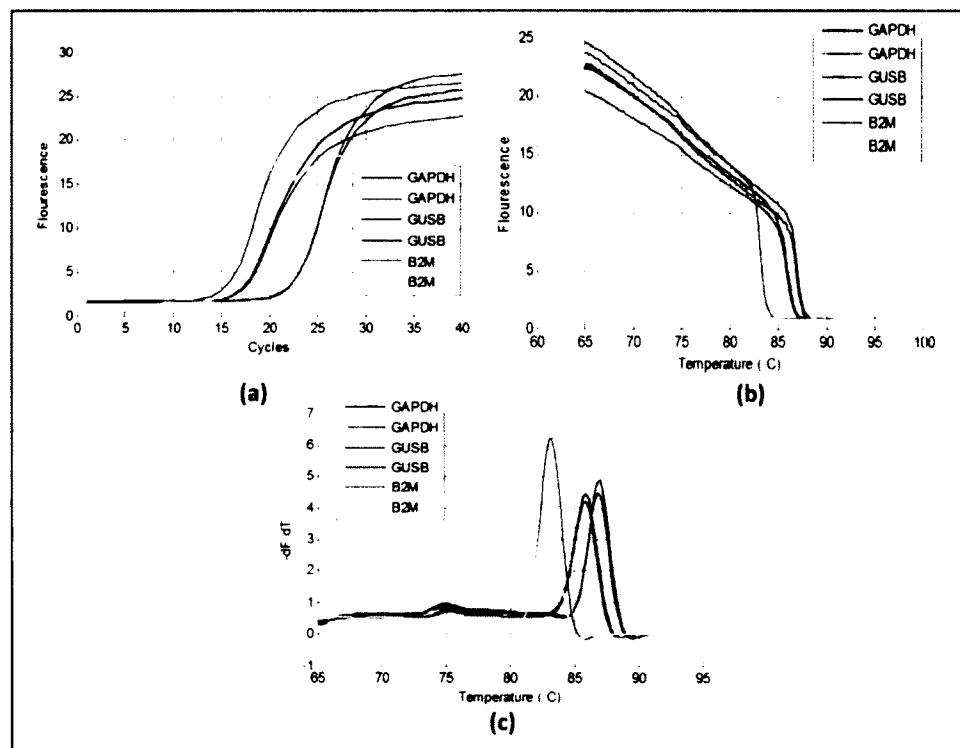
### 2.4.3 Optimization of RT-PCR for On-chip Detection

Reverse transcription PCR (RT-PCR) involves reverse transcription of RNA to complementary DNA (cDNA), followed by amplification with PCR. Critical factors that must be optimized for fast and quantitative analysis of RNA via RT-PCR in lab-on-chip devices are:

- 1) Speed of analysis: Reverse transcription requires an incubation time of 5 min for successful conversion to cDNA. PCR of cDNA also adds time to the analysis.
- 2) Sample lower limit: Concentration of initial sample needed for successful amplification.
- 3) Multiplex amplification for quantitative analysis.

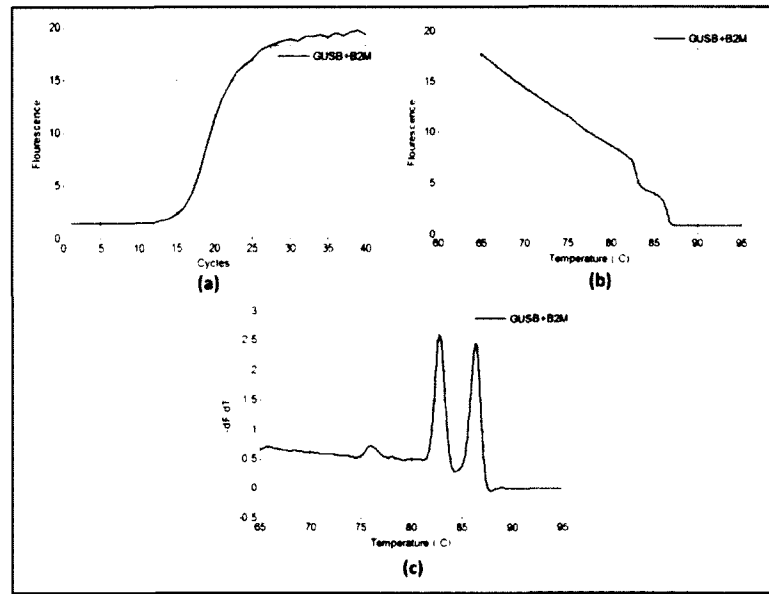
These parameters must first be optimized in a standard real-time PCR instrument to determine the performance limits of the RT-PCR.

Three individual primers for gene segments GAPDH, GUSB, B2M were used to amplify the commercial human RNA. 40 ng/ $\mu$ l of RNA concentration was used with the Takara kit protocol (**Table A-1**) in the Light Scanner system. Thermocycling protocols (**Table A-2**, **Table A-3**) for real-time PCR was determined based on the reaction type. **Figure 2-8** shows the amplification, standard melt, and melt peak curves for the three gene-specific primers. Melting temperatures obtained from a single experiment for individual primers B2M, GAPDH, and GUSB are 83.08°C, 85.87°C, and 86.95°C, respectively.

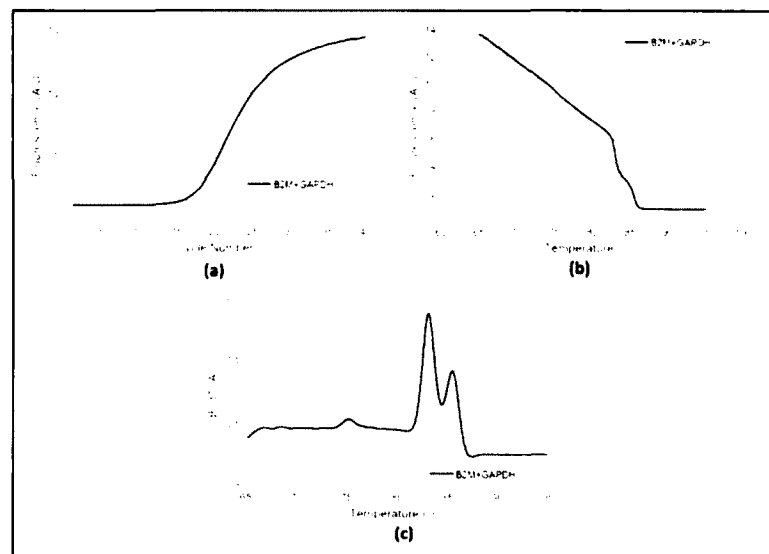


**Figure 2-8:** Amplification of RNA using individual primers (B2M, GAPDH and GUSB) and melt curve analysis in LS32 system. (a) Amplification curves, (b) Standard melt curves, (c) Melt peaks. Concentration of RNA used is 40 ng/ $\mu$ l. Reverse transcription time is 5 min and PCR hold times are 20 sec.

B2M and GUSB primers were amplified together in a single reaction mixture (Multiplex amplification). B2M and GUSB primers are chosen because their melting temperatures are 3.87°C apart. **Figure 2-9** shows the analysis of the B2M and GUSB multiplex amplification. Another combination of primer sets (B2M and GAPDH) was used to determine if they can be identified in a single RT-PCR process (**Figure 2-10**).

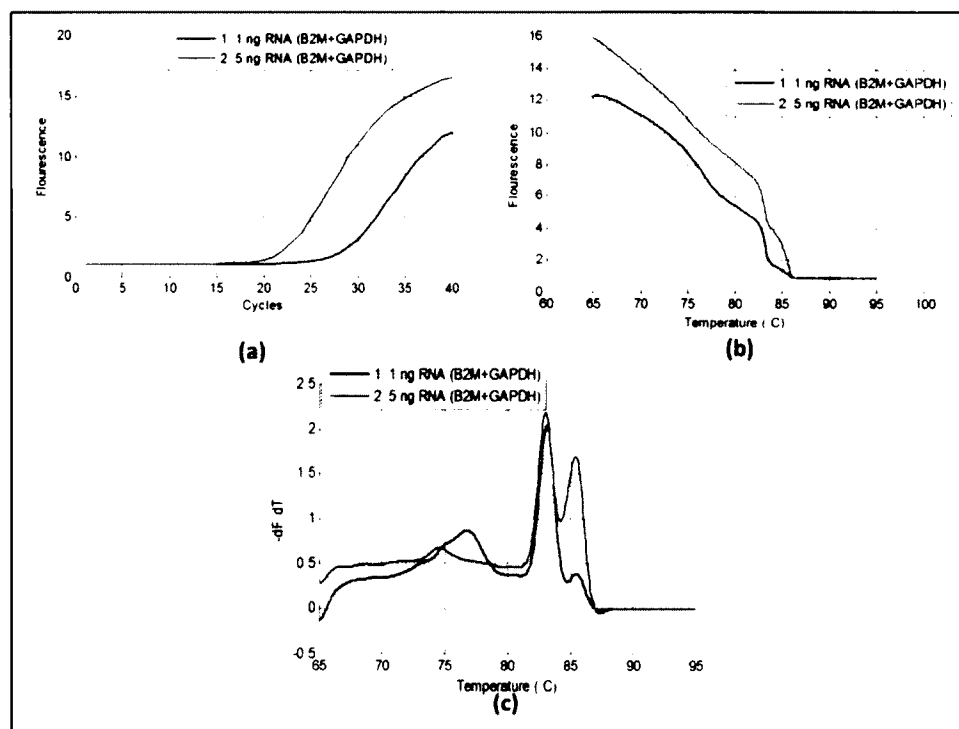


**Figure 2-9:** Amplification of RNA using multiple primers (B2M and GUSB) and melt curve analysis in LS32 system. (a) Amplification curves, (b) Standard melt curves, (c) Melt peaks. Concentration of RNA used is 40 ng/ $\mu$ l. Reverse transcription time is 5 min and PCR hold times are 20 sec.



**Figure 2-10:** Amplification of RNA using multiple primers (B2M and GAPDH) and melt curve analysis in LS32 system. (a) amplification curve, (b) standard melt curve, (c) melt peaks. Concentration of RNA used is 40 ng. Reverse transcription time is 1 min and PCR hold times are 0 sec.

Effect of RNA sample concentration on RT-PCR was determined by decreasing the concentration of RNA three orders of magnitude. When the concentration of RNA sample was decreased, amplification cycle was shifted, and GUSB gene target was not amplified. This effect is caused by the lower expression of the GUSB gene in the human RNA sample. Multiplex amplification using 1 ng/ $\mu$ l RNA sample concentration amplified both gene targets for analysis. RT hold time was also decreased to 1 min along with 0 sec PCR hold times ( **Figure 2-11**).



**Figure 2-11:** Amplification of RNA using multiple primers (B2M and GAPDH) and melt curve analysis in LS32 system. (a) Amplification curves, b) Standard melt curves, c) Melt peaks. Reverse transcription time is 1 min and PCR hold times are 0 sec.

In conclusion, RT-PCR performed with Takara's one-step SYBR PrimeScript kit using the Light Scanner system was successful. A lower detection limit of 10 pg RNA was detected with 5 min reverse transcription hold time and 20 sec PCR hold times. A lower of 1 ng RNA was detected with 1 min reverse transcription hold time and 0 sec PCR hold times. Combinations of two primer sets (B2M+GUSB and B2M+GAPD) were used together to perform RT-PCR successfully.

#### 2.4.4 Oscillating-flow RT-PCR

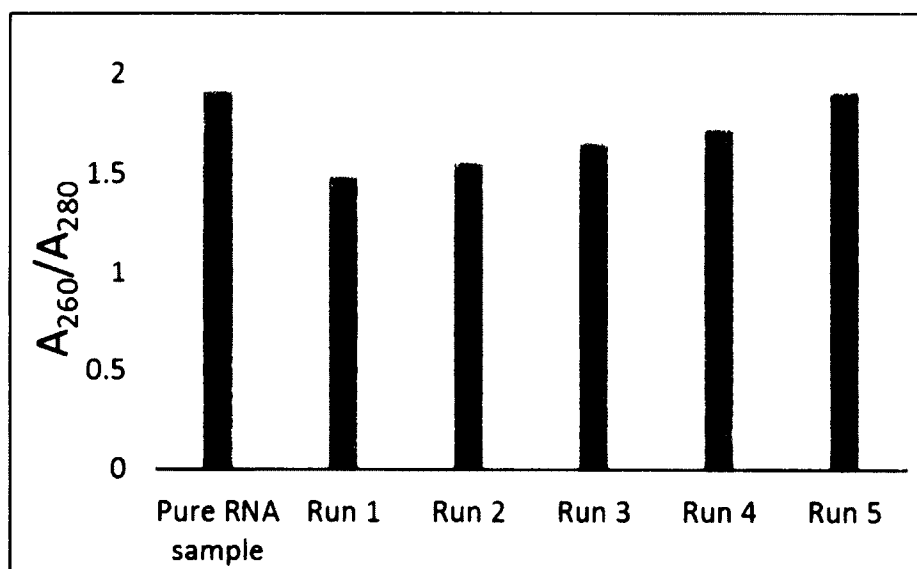
Reverse transcription PCR (RT-PCR) was also performed using the thermal gradient oscillating-flow PCR. Handling RNA for microfluidic PCR is difficult, as RNA is subjected to degradation easily. As the sample is subjected to many preprocessing steps such as sample preparation and loading, strict care must be taken in performing RT-PCR. After loading the microfluidic channel surfaces with RT-PCR sample reagents, RT on-chip is evaluated by determining the amplification efficiency.

##### 2.4.4.1 Demonstration of on-chip reverse transcription

For successful on-chip reverse transcription, RNA must not degrade during the preparation and sample loading into the microfluidic device. To evaluate degradation, the RNA in the sample is examined, after it has passed through the microfluidic device. with the Nanodrop instrument. The ratio of absorbances at 260 nm and 280 nm is a good indicator of RNA quality. The absorbance ratio ( $A_{260}/A_{280}$ ) of  $\sim 2$  is considered as standard quality measure for pure RNA. RNA diluted in water (40 ng/ $\mu$ l final concentration) is passed through the microfluidic device and is collected for measuring absorbance. Several 20  $\mu$ l sample runs were performed to determine the saturation and integrity of RNA after passage through the chip. **Figure 2-12** shows the RNA quality for

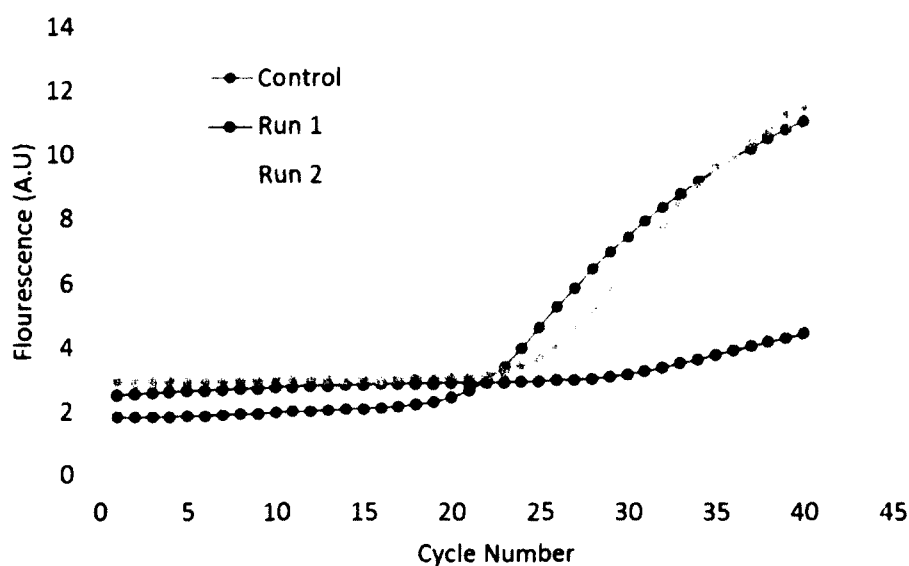


pure sample passed through the microfluidic chip. This indicated that several runs of RNA sample are required to saturate and obtain good quality RNA.



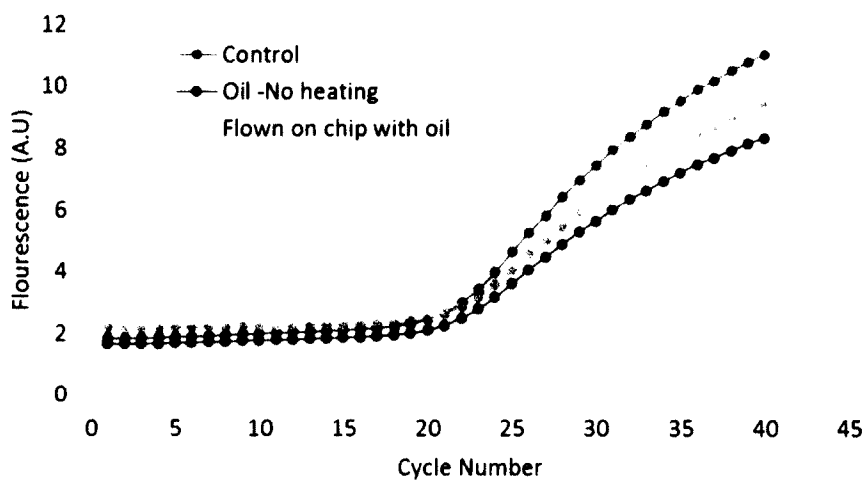
**Figure 2-12:** Effect of sample flow in the microfluidic device on  $A_{260}/A_{280}$  ratio for RNA quality.

Once the RNA quality is determined, the RT-PCR sample is passed through the microfluidic device and collected at the end to determine the saturation of RT-PCR reagents to the channel surface. Loss of reagents to the channel surface results in inefficient RT-PCR. The RT-PCR sample is passed through the chip and is collected. The collected samples are amplified in a real-time PCR instrument to determine amplification efficiency. **Figure 2-13** shows the amplification efficiency after several runs of the sample collected from the microfluidic device.

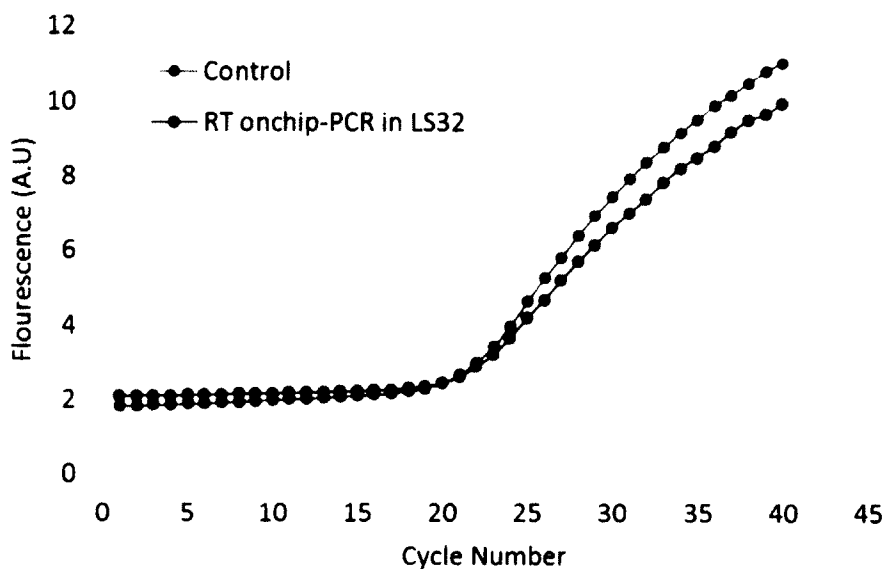


**Figure 2-13:** Effect of sample loading in the microfluidic device on RT-PCR efficiency.

In the oscillating-flow methodology, a sample plug was used within flourinert oil. The effect of oil on RT-PCR efficiency was also determined. After ensuring that all steps are compatible for RT-PCR in the microfluidic device, the sample is filled in the channel for reverse transcription. The temperature of the microfluidic device is set at 50°C to perform reverse transcription on-chip. The sample is left at this temperature for 5 minutes and collected to perform PCR in the real-time instrument. **Figure 2-14** shows the amplification curves for control sample that is amplified with reverse transcription and PCR steps in a real time instrument, and the sample with reverse transcription step performed on-chip (**Figure 2-15**) and PCR performed in real-time instrument.



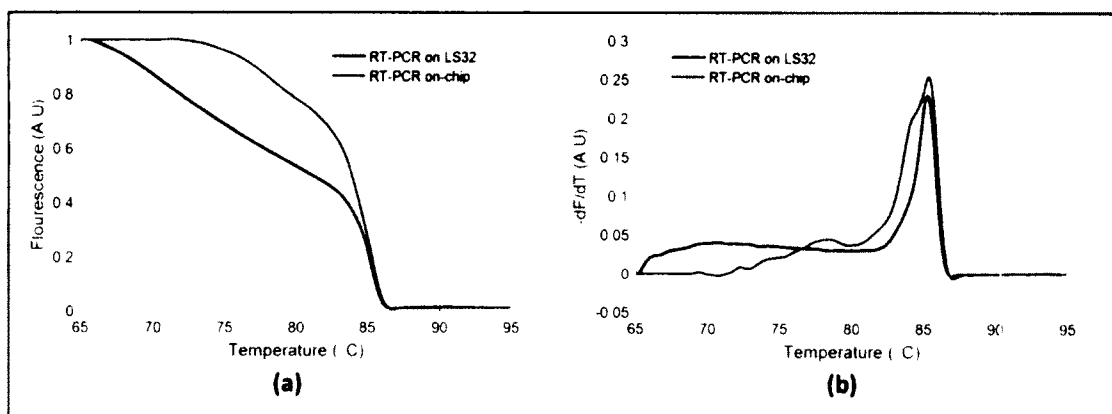
**Figure 2-14:** Effect of sample interaction with flourinert oil on RT-PCR efficiency.



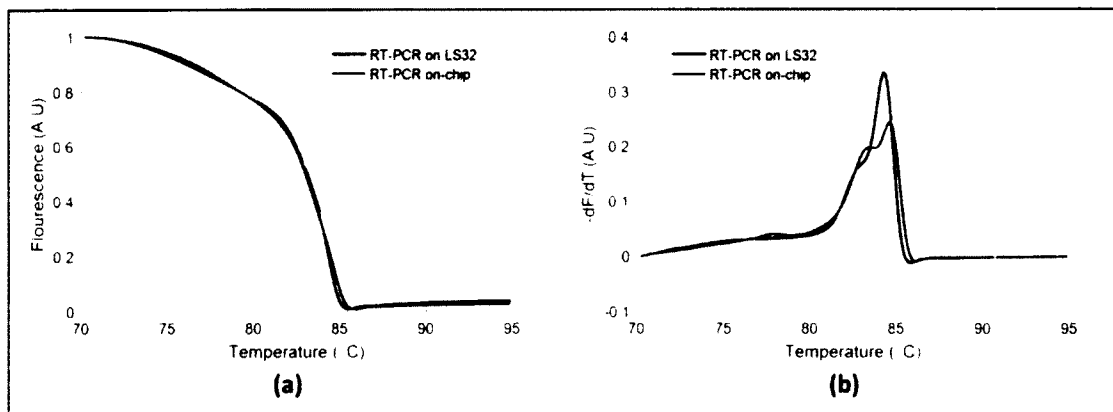
**Figure 2-15:** Comparison of on-chip reverse transcription to real-time PCR instrument. Incubation time for reverse transcription is 5 min in both cases. PCR is performed in the real-time instrument after on-chip reverse transcription.

#### 2.4.4.2 On-chip RT-PCR

Reverse transcription PCR was performed in the oscillating-flow PCR system (**Figure 2-2**). The RT-PCR sample is first loaded into the microfluidic device, and the controller is used to raise the temperature of the device to 50°C. The sample is incubated for 5 min for reverse transcription of RNA to cDNA. Then the sample is oscillated between the denaturing and annealing temperatures for performing PCR. After thermocycling for 40 cycles, the sample is collected from the microfluidic device and is melted in the light scanner LS32 system. **Figure 2-16** shows the standard melts when compared to sample amplification in LS32. High resolution melts are also compared for both the standard LS32 system and the developed oscillating-flow system (**Figure 2-17**).



**Figure 2-16:** (a) Standard melt curves after RT-PCR in LS32 and in the developed oscillating-flow system. (b) First order derivatives of the standard melts for melting temperature analysis.



**Figure 2-17:** (a) High-resolution melt curves after RT-PCR in LS32 and in the developed oscillating-flow system. (b) First order derivatives of the high-resolution melts for melting temperature analysis.

## 2.5 Conclusion

Oscillating-flow thermal gradient system for nucleic acid amplification is developed for simultaneous amplification and melting analysis. Both DNA and RNA were amplified and analyzed using the developed system. Oscillating-flow methodology was implemented in the thermal gradient system to achieve nucleic acid amplification. The developed thermal gradient oscillating-flow system has many advantages over the current methods, such as cycle number flexibility, reduced cross contamination, and effective surface to volume ratio for reagent loss.

**CHAPTER 3**

**MICROFAB IN A MICROWAVE OVEN: SIMULTANEOUS  
PATTERNING AND BONDING OF GLASS  
MICROFLUIDIC DEVICES**

**3.1 Introduction**

For the past few decades, microfluidics has revolutionized the fields of biochemistry and biotechnology. Advances in the field have led to the development of lab-on-chip technology, which is aimed at combining several laboratory processes into a single chip. Historically, these devices were created from conventional microelectronics fabrication processes; therefore, silicon and glass substrates were most common. Such techniques generally required a cleanroom infrastructure, complex instruments, and harsh chemicals.

In recent years, effort has been made to develop less complex microfluidics fabrication methods. This has led to the emergence of polymers such as polydimethylsiloxane (PDMS) [9], cyclic olefin polymers (COP) or copolymers (COC) [46], [47], and polymethylmethacrylate (PMMA) [48] as microfluidic device materials [11]. While the primary thrust has always been cutting-edge research, there is significant interest in moving away from highly specialized materials, equipment, and infrastructure to manufacture or prototype microfluidics. For example, the Khine research group at University of California, Irvine made significant advances in microfluidics and

nanotechnology using a children's toy, Shrinky Dink [13], [14], [49]; the Andrade research lab at University of Utah demonstrated how a hobby-grade vinyl sign cutting plotter could be used to make high-precision microscale structures and microchannels [10]; and the Whitesides lab at Harvard pioneered the use of ordinary paper as a platform for microfluidic assays [12]. This article presents a microfabrication development in this same vein. A microwave kiln, marketed as a hobby-grade tool for jewelry making, is used here to fabricate all-glass microfluidic devices. Internal temperatures rise above 800°C in less than 3 minutes and microchannel fabrication and fusion bonding is performed nearly two orders of magnitude faster than conventional methods.

Conventional methods to fabricate glass microfluidic channels include surface micromachining, buried-channel micromachining, and bulk micromachining[18]. These methods use complex lithography techniques to pattern and etch glass substrates to form microfluidic structures and channels. Regardless of the fabrication method used, the last process in the fabrication sequence involves some type of laminate bonding to yield closed fluidic paths. Traditional techniques widely used to seal glass microchannels to either glass or other substrates are glass fusion bonding and anodic bonding of glass to silicon[18].

Alternatives have been explored, and some room temperature bonding techniques have been invented. For example, Qun Fang *et al.* [50] have developed a method for room temperature bonding of glass substrates that can be achieved by soaking the substrates in concentrated sulphuric acid ( $H_2SO_4$ ) for 12 hours and squeezing the substrates together with high pressure. Also, Luo *et al.* [51] improved the process of bonding glass substrates using  $H_2SO_4$  cleaning by an additional HF stream to form a thin

hydrolyzed water layer between the surfaces, which provides enhanced bonding strength and quality. Furthermore, a combination of reactive ion etching (RIE) plasma treatment with a variety of gas sources such as oxygen/tetrafluoromethane ( $\text{CF}_4$ ) has been investigated for room temperature bonding of glass substrates with micro and nano channels [19], [52], [53]. Such next-generation bonding methods have decreased process times and improved feature resolution. However, they generally require advanced equipment and infrastructure.

To overcome some of the complexity in conventional fabricating all-glass microfluidic devices, glass composite devices have been developed. Composite devices gained popularity because of they are simple to fabricate and do not require a cleanroom environment. For example, xurography [10] has been used to pattern double-sided tapes which serve as both a bonding and channel layer between un-patterned glass blanks [45], [54]. Also, PDMS bonding to glass with plasma treatment [15] has shown promise for the wide adaptation of composite devices. Although glass composite devices have advantages over their polymer counterparts (e.g. broad spectrum optical transparency), fused-glass microfluidic devices have added versatility, such as high temperature stability, pressure rating, solvent compatibility, and well-established surface modification methods for immobilization or passivation.

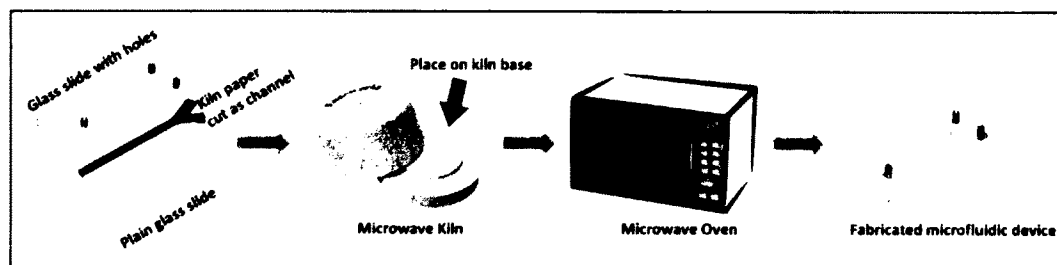
In this article, we present a new method for the simple and rapid fabrication of glass microfluidic devices. The proposed method is based around a one-step technique that simultaneously forms the microchannels in the glass and bonds the layers together. Glass fusing is a common crafting technique for artists and hobbyists, which involves melting two or more compatible glass pieces at high temperatures in a kiln. Compatible



glass pieces with the same coefficient of expansion (COE) and viscosity are generally used in glass fusing and which are melted at temperatures typically in the range of 590°C to 870°C. We report the rapid fabrication of glass microfluidic devices by glass fusing technique in a microwave oven using a commercially available kiln.

### 3.2 Materials and Methods

Fabrication of microfluidic devices (**Figure 3-1**) using the proposed study involves the following steps. (1) Positioning of the template between the glass slides, (2) Placement of the slides in the kiln, (3) Heating of the kiln in the microwave oven, (4) post-processing of the microdevice.



**Figure 3-1:** Schematic of the fabrication process.

#### 3.2.1 Glass Preparation

Selection of glass for this technique requires matching the coefficient of expansion (COE). Glass with identical COE is used for fusing in this study. Glass types such as fusible glass (Diamond Tech, FL, USA., 90 COE; thickness – 2 mm), Spectrum® glass (Spectrum® Glass Company, USA., 96 COE; thickness – 2 mm), soda lime glass (Fisher Scientific, MA, USA., 104 COE; thickness – 1 mm), and borosilicate glass (Bullen Ultrasonics, OH, USA., 33 COE; thickness – 2 mm) were used to evaluate the

fabrication technique. Glass sheet is cut into 25 mm × 75 mm pieces using diamond tipped glass cutter. A Dremel tool is used to drill holes into the glass according to the channel geometry for inlet and outlets, as described previously [45]. Cleaning of the glass pieces prior to the device fabrication was performed by washing with 1% solution of detergent (Alconox, NY, USA), then with distilled water and were dried with compressed air.

### 3.2.2 Channel Design

The microfluidic channel design can consist of high-aspect ratio regions with a rectangular cross-section and thin channel regions with a circular cross-section. Channel geometries for rectangular cross-sections were designed to fit the glass pieces and were drawn in Adobe Illustrator (Adobe Systems, CA, USA). Since the technique is based on glass fusing at high temperatures, the sacrificial layer between the glass pieces (around which the softened glass will mold) should withstand high temperatures. Ceramic-impregnated fiber paper is ideal for this application. It is commonly used to protect kiln walls from molten glass and dust. The fiber paper is ceramic-impregnated with an organic rigidizer which, when fired, turns black and then white again when the binder burns off. For this project, a cutting plotter (Graphtec America Inc., USA) was used to cut kiln fiber shelf paper (Bullseye Glass Company, USA., thickness -130 μm) into the desired channel geometry, according to the method described previously [45]. To obtain channels with circular cross-section, the design was laid out in kiln thread (diameter -800 μm), which was obtained by separating the strands of kiln rope (DelphiGlass, USA).

### 3.2.3 Assembly and Fusing

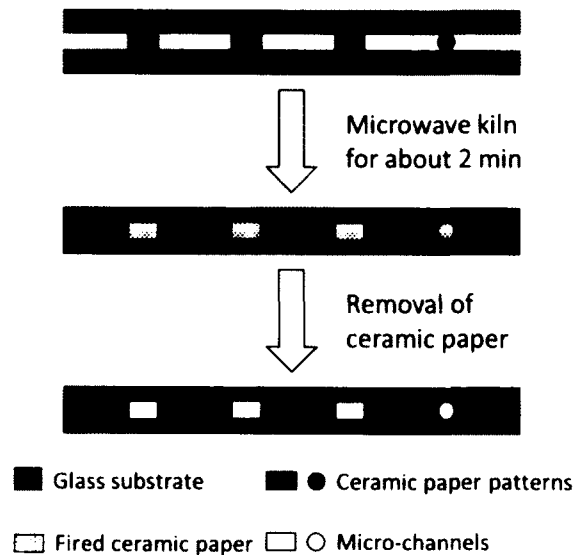
Holes drilled in the top glass piece are plugged using kiln rope. The channel cut out of the kiln paper was sandwiched between a plain glass piece and glass piece with holes plugged with fiber rope. This sandwich is placed inside the Fuseworks™ Microwave Kiln (Diamond Tech, USA) which is placed within a household-style microwave oven. For the testing conducted as part of this work, an 1100 W microwave oven was used at full power. Firing time in the microwave oven must be optimized for glass thickness and microwave power output. The manufacturer provides a suggested starting point for the firing time for a ¼ inch thick glass for different microwave power wattage (**Table 3-1**). When bombarded with microwave radiation, the proprietary coating on the inner surface of the Fuseworks™ Microwave Kiln reaches temperatures between 760°C to 870°C. When softened, the glass pieces mold around the patterned paper (as it oxidizes) and fuses together, thereby forming the designed flow channel.

**Table 3-1:** Dependence of firing time on microwave power.

<b>Microwave Power (Watts)</b>	<b>Firing time (minutes)</b>
800	3 to 4
1100	2 to 3.5
1200	2 to 3.5

### 3.3 Experimental Preparation

After firing, the kiln is then removed from the microwave and is placed on a heat resistant surface to cool for at least 45 minutes. The microfluidic device is cleaned with a pressurized air gun and placed in an ultrasonicator (B200, Branson Ultrasonics Corp, USA) for 5 min to 20 min, depending on the geometry, until the fired kiln paper is removed (**Figure 3-2**). After the glass is cleaned and dried, blunt tip luer-lock needles (NicVape, SC, USA) is attached with instant adhesive (Loctite® 460, OH, USA) to the inlet and outlet ports on the microfluidic devices. Tubing is connected to the access ports through fluidic interconnects (IDEX Health & Science, WA, USA) to allow fluid flow into the fabricated microfluidic devices. Syringe pumps (Pump11 Elite, Harvard Apparatus, USA) were used to introduce fluids into the devices. An optical microscope was utilized to image the flow in the devices.



**Figure 3-2:** Schematic showing the simultaneous fabrication of glass microchannels and fusing with ceramic impregnated paper.

### 3.4 Results and Discussion

#### 3.4.1 Firing Time

Time in the microwave oven, firing time, is key. A difference of just a few seconds can have a significant impact. If the firing time is too long, the glass will lose its form, and the sacrificial material for the channel may even migrate through the liquefied glass. If the firing time is too short the glass pieces do not adequately fuse. The firing time was optimized for several glass types and dimensions by examining the glass bonding interface and the channel distortion after fusion. **Table 3-2** gives these optimum firing times for an 1100-watt microwave for different types of COE glass and thicknesses.

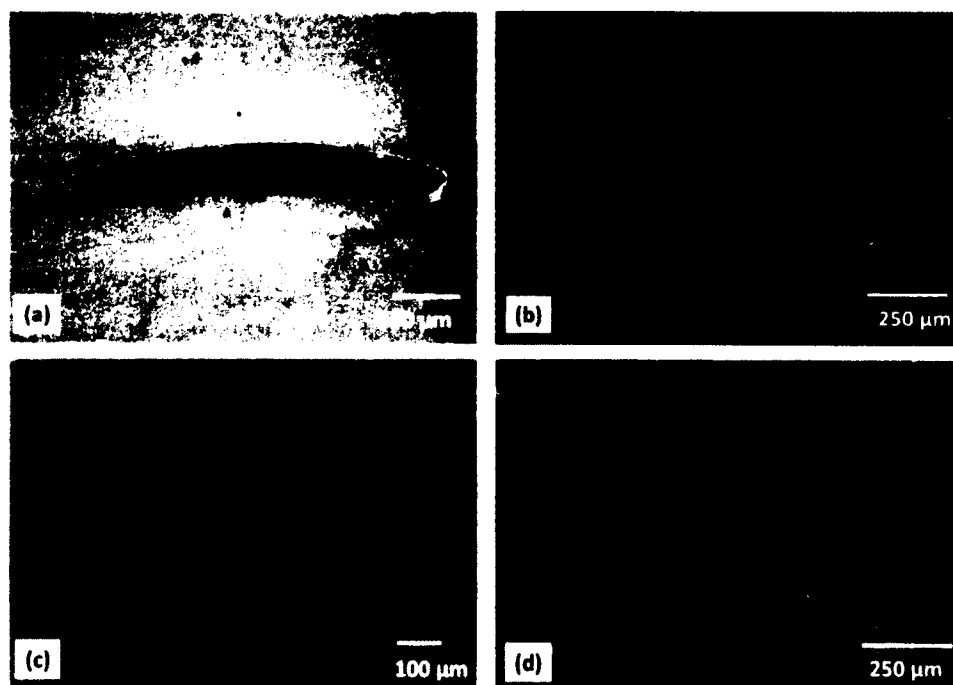
**Table 3-2:** Firing time for different COE glass.

Glass type / thickness	COE	Firing time (min:sec)
Borosilicate / 2mm	33	3:30
Fusible glass / 2mm	90	3:00
Spectrum clear / 2 mm	96	2:00
Soda lime glass / 1mm	104	1:45

#### 3.4.2 Microfluidic Channels

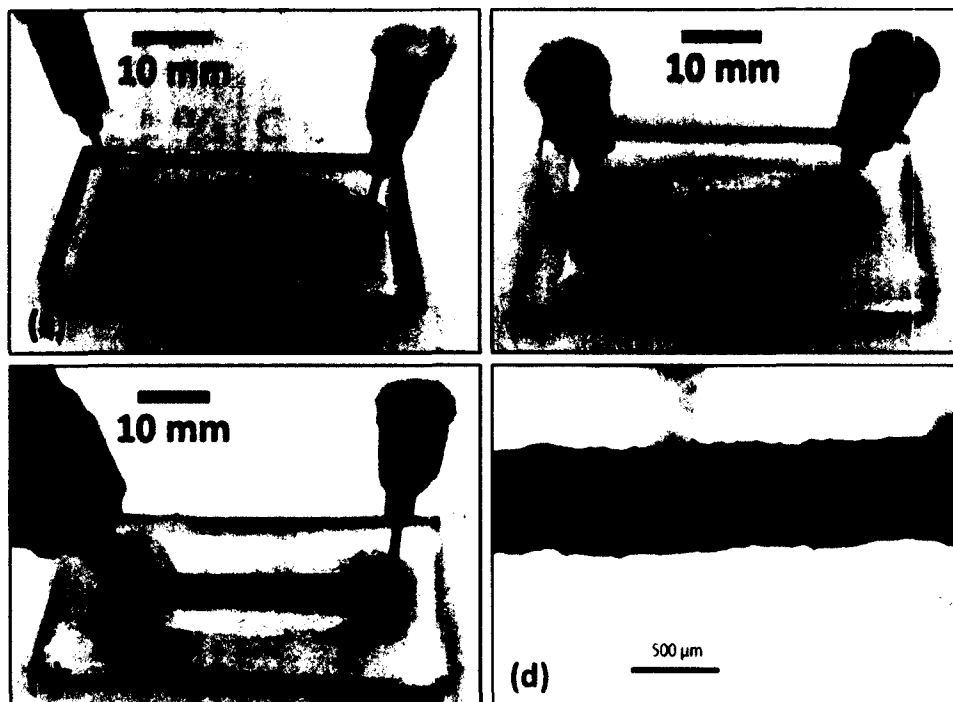
Microchannels with rectangular and circular cross-sections (**Figure 3-3**) were fabricated using the method explained above. The patterned kiln paper was used as the sacrificial layer to produce the rectangular cross-section channels, and kiln thread for the circular cross-sections. The microchannel walls in these devices possessed a unique

texture caused by the roughness of the sacrificial material. The ability to create high-aspect ratio rectangular and circular channels with a simple process is a strong advantage of this technique. Fabrication of the microchannels and bonding is achieved in 2 minutes to under 4 minutes (**Table 3-2**), depending on the glass type and thickness. The entire fabrication process from concept to device takes about an hour, estimating 5 minutes for cutting the paper pattern, 4 minutes for firing in the kiln (assuming 2 mm thick borosilicate glass), 45 minutes for cooling in the kiln after the firing in the microwave oven, and 5 minutes for ultrasonication and cleaning. Channel widths as small as 500  $\mu\text{m}$  were successfully produced in this study.



**Figure 3-3:** SEM micrographs of the fabricated microfluidic channels a) cross-section of a straight rectangular channel, b) surface roughness of the channels, c) cross-section of a circular channel, d) surface roughness of the fired ceramic impregnated paper.

In general, feature size is limited by the sacrificial material used for patterning by cutting plotter. Features that are taller than their width are difficult to cut using the cutting plotter, and generally widths twice the height of the material are preferred. This technique is similar to soft-lithography, which uses a mold – patterned in the negative shape of the desired feature – to form the shape of the substrate material. In this work, though, it is softened glass that forms around the paper template (**Figure 3-2**). However, soft lithography has separate processes for the patterning of the material and the subsequent bonding of the layers to form the channels. In contrast, using this technique, the channels are formed around the paper mold and the glass layers are fused together in a single process. Since the glass is melted and fused in this technique, the pressure resistance for fabricated microfluidics devices is only limited by the fluidic connects. The microfluidic devices produced using this technique are all-glass. They are compatible with most chemicals. We have demonstrated the fabrication of different channel geometries using the proposed technique (**Figure 3-4**). The developed technique is believed to be used by the research community to demonstrate a quick and proof-of-concept of their research that require glass microfluidics. Microfluidic devices were fabricated using different channel geometries and are tested for performance.



**Figure 3-4:** Microfluidic devices with different flow geometries. a) S-shaped channel, b) straight channel, c) Y-shaped channel, d) smallest feature size channel fabricated using this study. Red and green dyes are used for flow demonstration.

### 3.5 Conclusion

The article presents a simple technique for the rapid fabrication of glass microfluidic devices. A hobby-grade kiln is used in a conventional microwave oven to soften the glass layers such that they mold around a sacrificial layer and fuse together. This technique has been demonstrated here for both rectangular and circular cross-section channels, and for dimensions as small as 350  $\mu\text{m}$ . For the glasses evaluated in this study, formation of the channels was achieved within 4 minutes or less. Both the rapidity of the process and the simultaneous nature of the patterning and bonding that occurs represent a significant improvement beyond conventional methods for all-glass microfluidic device fabrication.



## CHAPTER 4

### MICROSCALE THERMAL BIOSENSOR: CRITICAL DESIGN CONSIDERATIONS AND OPTIMIZATION

#### 4.1 Introduction

Calorimetric biosensors have been used to detect various bioprocesses such as enzyme-substrate activity, protein binding activity, DNA reactions, and cell metabolism. Microscale calorimeters were developed in recent years for their advantages in sample handling, speed of detection, and sensitivity. Several thermal sensors such as thermistors, thermopiles and RTD's were used in calorimetric biosensors to convert the universal nature of heat power production of biochemical reactions to a measurable output. Thermopiles are versatile thermal sensors for microscale chemical detectors because they have high common mode thermal noise rejection ratio and can be easily miniaturized. They have been used for biological reagent detection and chemical analysis. For example, Baier *et al.* developed a microcalorimeter with bismuth (Bi)-antimony (Sb) thin film thermopiles to detect the exothermic reaction of oxidation of ascorbic acid by ascorbate oxidase [55]. Lerchner and colleagues applied the same method for the measurement of oxidation of glucose by glucose oxidase/catalase [56], metabolic dynamics of biofilms in real-time [57], and hybridization of single stranded DNA strands [58]. More recently, Guilbeau *et al* developed thermopile-based sensors for the detection of glucose [59], L-glutamate [60], and DNA sequencing [61]. The majority of the microcalorimeter

applications were proof-of-concept in nature, but they have strong potential for development for clinical, scientific, or commercial need. Success of these emerging experimental methodologies will be determined by such factors as the sensitivity and speed of these analyses when compared with existing technologies. These performance metrics are fundamentally related to the thermal transport through the microsystems.

A critical element of thermopile function is the thermal separation between the measuring and reference junctions. One common method has been to divide the devices into separate reaction chambers [62] or flow streams [63]. While this configuration thermally isolates the two regimes from each other effectively, it also sacrifices some of the common mode rejection potential of thermopiles. For example, ambient temperature gradients will impact measuring and reference areas that are spaced far apart. Other unavoidable experimental inconsistencies, such as variations in pressure drop or flow control within the two regions, can create artifacts in measured signals. In response, researchers have created measuring and reference regions within the same flow channel [64] or sample chamber [65]. In such systems, two approaches can be used to direct the heat signal to the measuring junctions and isolate the measuring and reference junctions:

1. Controlled symmetry of heat generation by virtue of selective surface preparation.

A promising example of this approach is the localized immobilization of reactants within a single flow channel.

2. Heat generation at the interface of two fluid streams. In such a configuration, the location of the fluidic interface is used to direct the heat flow. In this latter method, the isolation of the heat and the resultant sensitivity of the thermopile

measurements are heavily determined by such factors as flow rate and fluidic positioning within the microchannel.

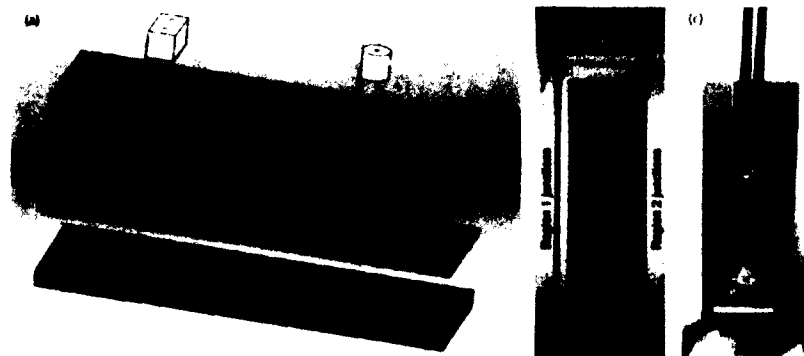
In this study, we characterize the impact of such critical parameters and provide some essential guidelines for the optimization of continuous flow systems in general. We have characterized the impact of flow velocity on the thermal time constant of the micro calorimeter, steady state response of the system, and the location of the sensor in the flow stream and provide essential guidelines for the optimization of single-stream thermopile systems.

## 4.2 Experimental Methods

The experimental setup for performance testing consists of a microfluidic chip with integrated thermal sensor, syringe pumps, nanovoltmeter and a computer for data analysis. Syringe pumps are used to drive the analytes through the microfluidic calorimeter. The exothermic reaction generated by the mixing of analytes in the microfluidic calorimeter is detected by the thermopile and a proportional voltage is recorded.

A micro-calorimeter is fabricated using a rapid prototyping technique called xurography [10]. The calorimeter consists of a 100  $\mu\text{m}$  deep Y-shaped channel microfluidic device, which is made by sandwiching a microscope glass slide (thickness–1.2 mm and thermal conductivity– $1.05 \text{ W (m}^\circ\text{C)}^{-1}$ , Electron Microscopy Sciences, Hatfield, USA), dual side adhesive Kapton® tape (KaptonTape.com), cut in the form of channel using a cutting plotter (Graphtec America Inc., USA) and a microscope glass coverslip of thickness–0.13–0.17 mm and thermal conductivity– $1.14 \text{ W (m}^\circ\text{C)}^{-1}$  (Electron Microscopy Sciences, USA). Bismuth (Bi)- antimony (Sb) thin film thermopile

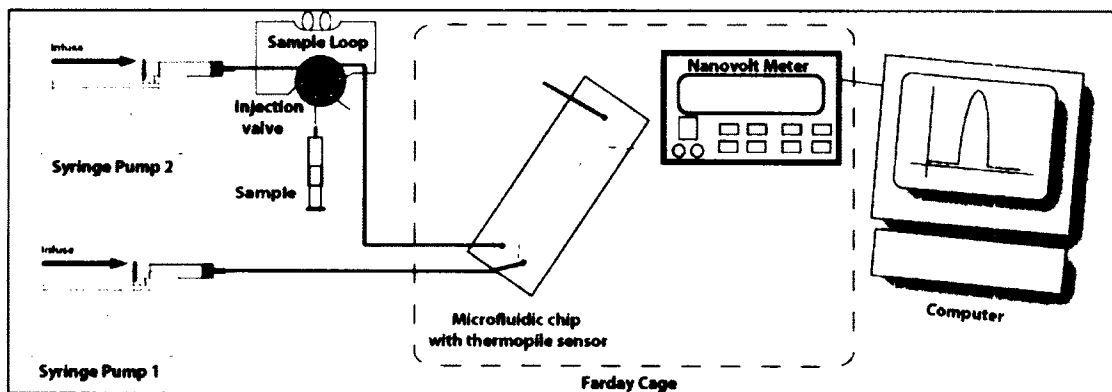
is integrated on the outer wall of the microscope glass coverslip. **Figure 4-1a** shows the schematic of the microfluidic device assembly. The thin film thermopile is fabricated on a 50  $\mu\text{m}$  polyimide (Dupont, USA) support using a thermal evaporation technique detailed by Guilbeau *et al.* [61]. Two shadow masks with complementary patterns are used to deposit bismuth and antimony metal layers on the polyimide support. First, a 0.8  $\mu\text{m}$  thick bismuth film is deposited onto the polyimide support using a shadow mask, and 1.2  $\mu\text{m}$  thick antimony film was evaporated onto Kapton using the shadow mask with a complementary design. **Figure 4-1b** shows the fabricated thermopile on a polyimide support. The thermopile is 3 mm wide by 6 mm long and has 50 thermocouple junctions with a theoretical Seebeck coefficient of  $5.95 \mu\text{V}(\text{mK})^{-1}$ . The thin film thermopile fabricated on polyimide support is integrated on to the microfluidic device using superglue. Conductive silverprint (GC Electronics, USA) was placed on the thermopile contacts and thin copper sheet (3M™ VHB™ Tape, 3M, USA) to provide electrical contact to the thermopile. The fabricated micro-calorimeter is shown in **Figure 4-1c**.



**Figure 4-1:** Fabrication of the micro-calorimeter. a) Schematic showing the fabrication of microfluidic device (not drawn to scale). b) Bismuth (Bi)- antimony (Sb) thin film thermopile fabricated on a 50  $\mu\text{m}$  polyimide support. c) Micro-calorimeter: microfluidic device with integrated thermopile.

### 4.3 Experimental Setup

Experimental setup used in this characterization study is shown in **Figure 4-2**. The entire setup is placed in a Faraday cage to reduce the noise interference with the recording system. To isolate the temperature field within the microcalorimeter from the surroundings, the device was placed within an enclosure. Two syringe pumps (Pump11 Elite, Harvard Apparatus, USA) are used to introduce water (house Deionized (DI) source) and ethanol (Ethyl Alcohol Pure 200 Proof, EMD Chemicals Inc., USA) continuously into the experimental device. A voltmeter (Nano-voltmeter 34420A, Agilent, USA) measures the thermopile output, which is recorded into a computer through a LabView SignalExpress interface (National Instruments, USA).



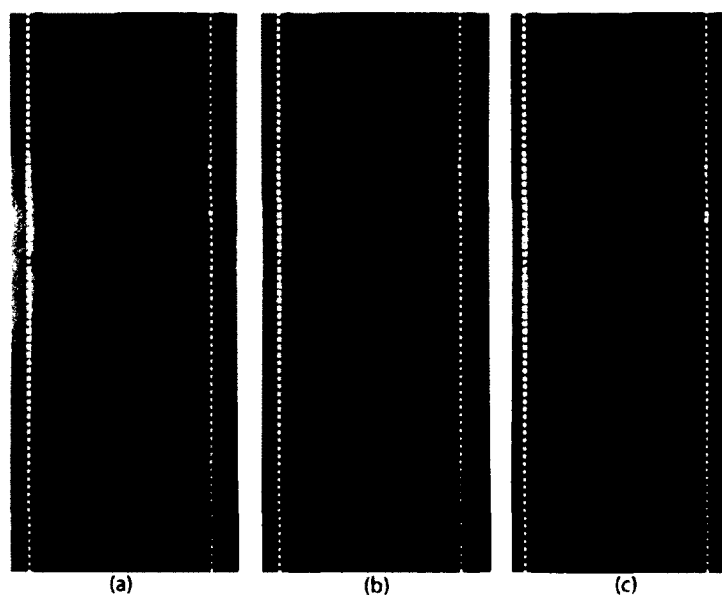
**Figure 4-2:** Schematic of the experimental setup.

### 4.4 Experimental Procedure

Two categories of experiments were performed: continuous and bolus mixing of water and ethanol.

#### 4.4.1 Continuous Mixing/Steady State Response

Continuous mixing of ethanol and DI water is used to characterize the steady state performance of the system. Syringe pumps are programmed to change the ratio of flow rates in inlet 1 and 2, respectively. The ratios are changed to move the mixing interface from the center to the edges of the channel where the thermopile junctions underneath are located. Several volumetric flow rates with varying flow ratios were used to characterize the steady state response. The microfluidic device at the different flow rate ratios indicates the mixing interface as shown in **Figure 4-3**.



**Figure 4-3:** Fluid flow in the micro-calorimeter showing mixing interface for different flow rate ratios. Dashed white lines represent the walls of the microfluidic device. The dashed red line represents the interface between the fluids driven through inlet 1 and 2. DI water is driven into one inlet, and DI water mixed with green dye is driven into the other inlet. a) Flow rate ratio 1:1 b) flow rate ratio 2:1 and c) flow rate ratio 4:1.

#### 4.4.2 Bolus Mixing

Mixing of a bolus sample is also studied, as in practical applications; the sample used for detection is limited by volume and cost. An injection valve (Rheodyne® Model

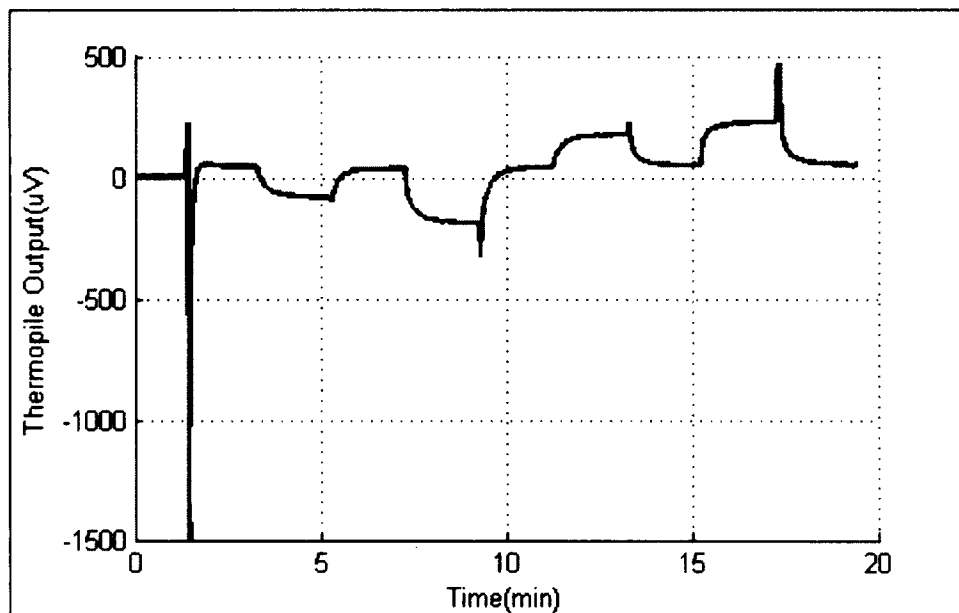
9725 Injector, Chrom Tech, Inc., USA) is used to inject a 5  $\mu$ l ethanol sample as a bolus into one of the inlets, while continuously pumping DI water in both the inlets. The mixing interface is adjusted so that it is positioned on one of the junctions of the thermopile. Several volumetric flow rates were used to study the response of the thermopile.

## 4.5 Results and Discussion

### 4.5.1 Experimental

#### 4.5.1.1 Continuous mixing/steady state response

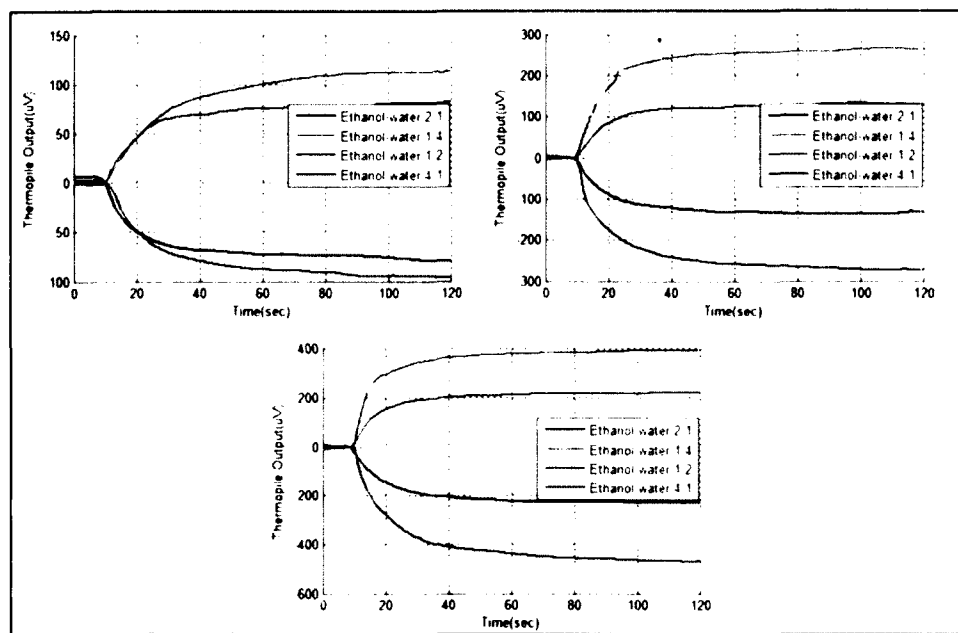
To characterize the performance of the micro-calorimeter, the heat released during the mixing reaction between water and ethanol was measured. The flow rates for the water and the ethanol streams were adjusted to change the location of the reaction zone relative to the measuring or reference junctions of the thermopile. The location of the fluid interface between the flow streams is a function of only the ratio of the flow rates. The nature of the mixing reaction, though, is additionally affected by the magnitude of those flow rates. The thermopile voltage responded sharply to changes in the reaction zone location. Flow rate ratios are programmed to move the interface from the center of the channel to either side of the channel. Three volumetric flow rates are used and the thermopile output is recorded. A typical recording of the thermopile output for the different ratios of the flow rates for a total volumetric flow rate of 200  $\mu$ l/min is shown in **Figure 4-4**. When the mixing layer is equidistant from the measuring and reference thermopile junctions, nearly zero voltage is transduced. The non-zero voltage indicated in **Figure 4-4** for a 1:1 ratio is from a slight thermal asymmetry caused by the unequal thermal conductivities of the two flow streams.



**Figure 4-4:** Thermopile output for different flow rate ratios for a total volumetric flow rate of 200  $\mu\text{l}/\text{min}$ . Syringe pumps are programmed to change the flow rate ratios from 1:1, 2:1, and 4:1.

Three total volumetric flow rates such as 100  $\mu\text{l}/\text{min}$ , 200  $\mu\text{l}/\text{min}$  and 400  $\mu\text{l}/\text{min}$  are imposed at different flow rate ratios. The thermopile outputs are plotted for different volumetric flow rates **Figure 4-5**. Analysis of steady state response provides the thermal time constant of the micro-calorimeter. First order derivatives represent the time constant analysis of the micro-calorimeter. The rise of the first derivate indicates how fast a steady state is achieved, and the fall indicates the thermal time constant of the system.

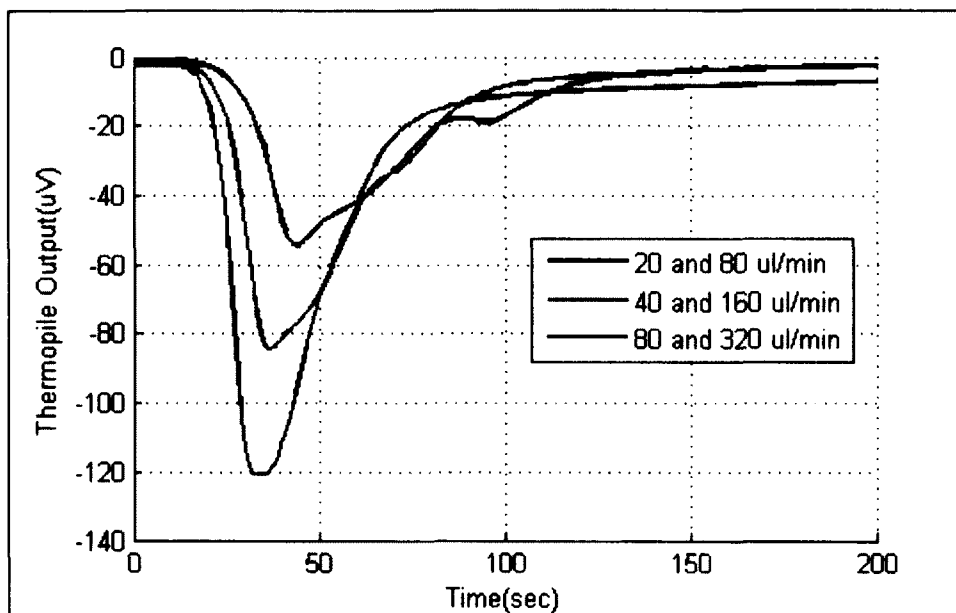




**Figure 4-5:** Steady state response of micro-calorimeter for different volumetric flow rates a) 100  $\mu\text{l}/\text{min}$ , b) 200  $\mu\text{l}/\text{min}$  and c) 400  $\mu\text{l}/\text{min}$ .

#### 4.5.1.2 *Bolus mixing*

Thermopile output for injection of a 5  $\mu\text{l}$  ethanol sample was recorded (**Figure 4-6**) for total volumetric flow rates of 100, 200, and 400  $\mu\text{l}/\text{min}$  in the microfluidic calorimeter. A flow rate ratio of 1:4 in the inlets is used for different total volumetric flow rates. When the ethanol sample is perfused over the thermopile junctions, the thermopile output changes because of the heats of mixing of ethanol and water. As the bolus sample passes over the thermopile junctions, the thermopile output reaches the baseline. The peak height of the signal represents the maximum change in the temperature detected by the thermopile, and the area under the curve represents the total heat detected for the bolus injection.



**Figure 4-6:** Thermopile output for a bolus injection of ethanol sample using an injection valve.

#### 4.6 Conclusion

The performance of the micro calorimeter was characterized by measuring the heat released during the mixing reaction between water and ethanol. The ratio of flow rates is adjusted to change the location of the reaction zone relative to the measuring or reference junctions of the thermopile. Analysis of steady state response provides the thermal time constant of microcalorimeter. As the flow velocity increases, the time constant to reach steady state response decreases.

## CHAPTER 5

### CONCLUSIONS

This research work focused on realizing technologies and methods towards an integrated lab-on-a-chip system for automated nucleic-acid analysis. This work has led to the development of novel microscale nucleic-acid amplification technique, a new simple method for the fabrication of all-glass microfluidic devices, and design considerations involved in the calorimetric sensing technology for a potential integration into lab-on-a-chip system for point-of-care applications. Each of these developments were demonstrated and characterized in this work.

Significant scientific research findings that have resulted from this work include the following:

1. **Oscillatory-flow thermal gradient PCR:** oscillatory-flow methodology was adopted to the thermal gradient system for spatial amplification of nucleic acid sample. This technique overcomes many existing limitations related to microscale continuous-flow PCR such as cycle number limitation, cross contamination. The method was suitable for the amplification of DNA and RNA without any additional temperature requirement for reverse transcription step in RNA amplification. Real-time analysis of nucleic acid sample for amplification and melting detection was performed using this system by recording and analyzing fluorescence images. Nucleic-acid amplification demonstrated in this work was achieved in 40 minutes.

2. **Simultaneous patterning and bonding of glass microfluidic devices in a microwave oven:** a novel and simple method was developed fabricated for the fabrication of microchannels and bonding to achieve microfluidic devices. A hobby-grade microwave kiln is used to obtain temperatures above 900°C for melting and fusing glass. A sacrificial layer (kiln paper) acts as a pattern and forms the channels in the glass-fusing stage. Rectangular and circular cross-section glass microchannels with a feature size of 350  $\mu\text{m}$  were fabricated through this technique. Research grade all-glass microfluidic devices were fabricated in under 4 minutes.
3. **Optimization of thermal sensing method for nucleic-acid detection:** thermal sensing of biochemical reactions is characterized for successful commercialization of this technology. Thermal signal response is based on the flow velocities and the thermal time constant of the system. Steady state responses are characterized to obtain maximum sensor output. The design considerations of the system and optimization parameters were identified to obtain maximum sensor output and to aid in successful integration of this sensing method for lab-on-a-chip automated analysis.

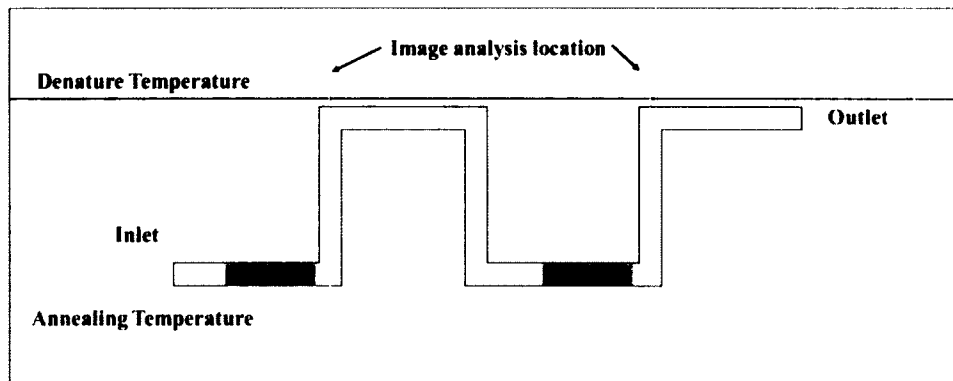
## CHAPTER 6

### FUTURE WORK

This section discusses the directions of future study that will provide potentially valuable insight towards lab-on-a-chip system for point-of-care applications.

#### 6.1 Quantitative Analysis

The microfluidic geometry used for oscillating-flow PCR in this work is a simple design. By changing the geometry (**Figure 6-1**) and repeating the design on the same chip, quantitative analysis can be performed. The standard PCR sample and the test PCR samples can be loaded with oil plugs in the system. When the PCR is performed using oscillating-flow, a single fluorescence image acquired can be used to quantitatively determine the difference between the standard and the test sample. By performing PCR using this technique, complexity related to multiplex analysis is eliminated.



**Figure 6-1:** Geometry for quantitative analysis.

## 6.2 Integration

Once the PCR is achieved, the system can be integrated with the thermoelectric sensor for on-chip detection. Symmetric PCR (equal concentration of primers) has been demonstrated in this dissertation, PCR variant such as asymmetric PCR can be performed to obtain one strand of target sequence in excess after the amplification. The amplified product can then be moved to the integrated thermoelectric sensor region to detect the amplified product. DNA hybridization reaction can be implanted over the thermoelectric sensor region to detect the amplified product. One advantage of using this approach is that the signal to be monitored is electrical, as opposed to optical. Only a voltmeter is required for such measurement, which provides an extremely simple way to fully automate the analysis system.

## **APPENDIX A**

### **RT-PCR EXPERIMENTAL PROTOCOL**

#### **A.1 Stock Solution Preparation**

The following steps are involved in the solution preparation:

1. Prepare the Forward and Reverse primers to 100  $\mu\text{M}$  stock and dilute to 10  $\mu\text{M}$ .
2. Prepare RNA to a stock concentration of 100 ng.

#### **A.2 One Step SYBR Prime Script RT-PCR protocol**

1. Prepare the following reagents on ice. < Per reaction >. **Table A-1** details the reagents list and concentrations for the preparing the mixture.

**Table A-1:** Reagents for one-step RT-PCR.

Reagents	Volume	Final Conc.
2X One Step SYBR® RT-PCR Buffer 4	10 µl	1X
PrimeScript 1 step Enzyme Mix 2	0.8 µl	
PCR Forward Primer (10 µM)	0.8 µl	0.4 µM <sup>*1</sup>
PCR Reverse Primer (10 µM)	0.8 µl	0.4 µM <sup>*1</sup>
Total RNA	2 µl	*2
RNase Free dH2O	5.6 µl	
Total	20 µl	

\* 1: The final concentration of primers can be 0.4 µM for most reactions. If this does not work, determine the optimal concentration within the range of 0.2 - 1.0 µM.

\* 2: It is recommended to use 10 pg - 100 ng total RNA as templates.

2. Start reaction Gently spin down PCR capillaries, then start the reaction after setting them in the LightScanner

Stage 1: Reverse transcription

42 °C 5 min. 20 °C/sec.

95 °C 10 sec. 20 °C/sec.

1 Cycle

Stage 2: PCR reaction

95 °C 5 sec. 20 °C/sec.



60 °C 20 sec. 20 °C/sec.

40 Cycle

Stage 3: melting curve analysis

95 °C 0 sec. 20 °C/sec.

65 °C 15 sec. 20 °C/sec.

95 °C 0 sec. 0.1 °C/sec.

**Note:** Heat inactivation prior to PCR should be 95 °C for 10 sec. There is no need to heat at 95 °C for (5-15 min). for initial denaturation, as is required for chemically modified Taq polymerase. If longer heat treatment is performed, the enzyme activity decreases and the amplification efficiency and the accuracy in quantification can also be affected.

3. Analyze after completion of reaction. After the reaction is completed, verify amplification curve and melting curve. Establish the standard curve when quantitative analysis is necessary.
4. Different thermocycling parameters for PCR are detailed in **Table A-2** and **Table A-3**.

### A.3 Shuttle PCR

**Table A-2:** Recommended shuttle PCR protocol for Takara kit.

Step	Temp.	Time	Detection	Remark
Denature	95°C	3 - 5 sec.	Off	Since the target size amplified for real-time PCR is generally shorter than 300 bp, denaturation at 95°C for 3 - 5 seconds is sufficient.
Annealing/ Extension	60 - 66°C	20 - 30 sec. (30 - 34 sec.) *1	On	Please try each standard protocol at first. The temperature should be optimized within the range of 60 - 66°C if optimization is required. When the reaction does not proceed efficiently, extend the time or change to a 3-step PCR protocol.

#### A.4 Three Step PCR

**Table A-3:** Recommended three step PCR protocol for Takara kit.

Step	Temp.	Time	Detection	Remark
Denature	95 °C	3 - 5 sec.	Off	Since the target size amplified for real-time PCR is generally shorter than 300 bp, denaturation at 95°C for 3 - 5 seconds is sufficient.
Annealing	55–60 °C	10 - 20 sec.	Off	Please try 55°C for 10 seconds first. When non-specific amplified products are generated or when the amplification efficiency is low, optimize the annealing temperature. Longer annealing time may sometimes improve the amplification efficiency.
Extension	72 °C	6 - 15 sec. (30 - 34 sec.) *1	On	When the amplified size is less than 300 bp, the time should be determined within the range of 6 - 15 seconds. Longer extension time can cause non-specific amplification.

Cycle: 30 - 45cycles

\* 1: Detection step must be set at more than 30 seconds for instruments of Life Technologies. For 7700 and 7500 Fast, it should be set at 30 seconds, for 7000 and 7300, at 31 seconds, and for 7500, at 34 seconds.

## BIBLIOGRAPHY

- [1] Delcan Butler, "Ebola experts seek to expand testing," *Nature*, vol. 516, pp. 154–155, 2014.
- [2] P. Nouvellet, T. Garske, H. L. Mills, G. Nedjati-Gilani, W. Hinsley, I. M. Blake, M. D. Van Kerkhove, A. Cori, I. Dorigatti, T. Jombart, S. Riley, C. Fraser, C. A. Donnelly, and N. M. Ferguson, "The role of rapid diagnostics in managing Ebola epidemics," *Nature*, vol. 528, no. 7580, pp. S109-16, 2015.
- [3] T. Houssin, J. Cramer, R. Grojsman, L. Bellahsene, G. Colas, H. Moulet, W. Minnella, C. Pannetier, M. Le Berre, A. Plecis, and Y. Chen, "Ultra-fast, sensitive and large-volume on-chip real-time PCR for the molecular diagnosis of bacterial and viral infections," *Lab Chip*, vol. 16, no. 8, pp. 1401–1411, 2016.
- [4] J. E. Hall, *Guyton and Hall Textbook of Medical Physiology: Enhanced E-book*. Elsevier Health Sciences, 2010.
- [5] Roland1952, "Comparison of a single-stranded RNA and a double-stranded DNA with their corresponding nucleobases," 2010. [Online]. Available: [https://commons.wikimedia.org/wiki/File:Difference\\_DNA\\_RNA-EN.svg](https://commons.wikimedia.org/wiki/File:Difference_DNA_RNA-EN.svg) [Accessed: 01-Jan-2016].
- [6] Enzoklop, "Schematic drawing of the PCR cycle," 2014. [Online]. Available: [https://commons.wikimedia.org/wiki/File:Polymerase\\_chain\\_reaction.svg](https://commons.wikimedia.org/wiki/File:Polymerase_chain_reaction.svg) [Accessed: 01-Jan-2016].
- [7] M. J. McPherson and S. G. Müller, *PCR*. Oxford: BIOS, 2000.
- [8] L. Kendall and L. Riley, "Reverse transcriptase polymerase chain reaction (RT-PCR)," in *Contemporary topics*, 2000.
- [9] D. C. Duffy, J. C. McDonald, O. J. A. Schueller, and G. M. Whitesides, "Rapid prototyping of microfluidic systems in poly(dimethylsiloxane)," *Anal. Chem.*, vol. 70, no. 23, pp. 4974–4984, 1998.
- [10] D. A. Bartholomeusz, R. W. Boutté, and J. D. Andrade, "Xurography: rapid prototyping of microstructures using a cutting plotter," *Microelectromechanical Syst. J.*, vol. 14, no. 6, pp. 1364–1374, 2005.
- [11] H. Becker and L. E. Locascio, "Polymer microfluidic devices," *Talanta*, vol. 56,

- no. 2, pp. 267–287, 2002.
- [12] A. W. Martinez, S. T. Phillips, M. J. Butte, and G. M. Whitesides, “Patterned paper as a platform for inexpensive, low-volume, portable bioassays,” *Angew. Chemie - Int. Ed.*, vol. 46, no. 8, pp. 1318–1320, 2007.
- [13] C.-S. Chen, D. N. Breslauer, J. I. Luna, A. Grimes, W.-C. Chin, L. P. Lee, and M. Khine, “Shrinky-Dink microfluidics: 3D polystyrene chips,” *Lab Chip*, vol. 8, no. 4, pp. 622–624, 2008.
- [14] A. Grimes, D. N. Breslauer, M. Long, J. Pegan, L. P. Lee, and M. Khine, “Shrinky-Dink microfluidics: rapid generation of deep and rounded patterns,” *Lab Chip*, vol. 8, no. 1, pp. 170–2, 2008.
- [15] S. Cosson, L. G. Aeberli, N. Brandenberg, and M. P. Lutolf, “Ultra-rapid prototyping of flexible, multi-layered microfluidic devices via razor writing,” *Lab Chip*, vol. 15, no. 1, pp. 72–6, 2014.
- [16] Y. Xia and G. M. Whitesides, “Soft lithography,” *Annu. Rev. Mater. Sci.*, vol. 28, no. 12, pp. 153–184, 1998.
- [17] A. Mata, A. J. Fleischman, and S. Roy, “Characterization of polydimethylsiloxane (PDMS) properties for biomedical micro/nanosystems,” *Biomed. Microdevices*, vol. 7, no. 4, pp. 281–293, 2005.
- [18] C. Iliescu, H. Taylor, M. Avram, J. Miao, and S. Franssila, “A practical guide for the fabrication of microfluidic devices using glass and silicon,” *Biomicrofluidics*, vol. 6, no. 1, pp. 16505–1650516, 2012.
- [19] Y. Xu, C. Wang, L. Li, N. Matsumoto, K. Jang, Y. Dong, K. Mawatari, T. Suga, and T. Kitamori, “Bonding of glass nanofluidic chips at room temperature by a one-step surface activation using an O<sub>2</sub>/CF<sub>4</sub> plasma treatment,” *Lab Chip*, vol. 13, no. 6, pp. 1048–52, 2013.
- [20] C. Zhang and D. Xing, “Miniaturized PCR chips for nucleic acid amplification and analysis: Latest advances and future trends,” *Nucleic Acids Res.*, vol. 35, no. 13, pp. 4223–4237, 2007.
- [21] F. C. Huang, C. S. Liao, and G. Bin Lee, “An integrated microfluidic chip for DNA/RNA amplification, electrophoresis separation and on-line optical detection,” *Electrophoresis*, vol. 27, no. 16, pp. 3297–3305, 2006.
- [22] J.-G. Lee, K. H. Cheong, N. Huh, S. Kim, J.-W. Choi, and C. Ko, “Microchip-based one step DNA extraction and real-time PCR in one chamber for rapid pathogen identification,” *Lab Chip*, vol. 6, no. 7, pp. 886–895, 2006.
- [23] M. U. Kopp, a J. Mello, and A. Manz, “Chemical amplification: continuous-flow PCR on a chip,” *Science*, vol. 280, no. 5366, pp. 1046–8, May 1998.

- [24] M. Hashimoto, P.-C. Chen, M. W. Mitchell, D. E. Nikitopoulos, S. a Soper, and M. C. Murphy, "Rapid PCR in a continuous flow device," *Lab Chip*, vol. 4, no. 6, pp. 638–645, 2004.
- [25] B. Shu, C. Zhang, and D. Xing, "A Handheld Flow Genetic Analysis System (FGAS): Towards Rapid, Sensitive, Quantitative, Multiplex Molecular Diagnosis at the Point-of-Care Level," *Lab Chip*, vol. 15, no. July 2016, pp. 2597–2605, 2015.
- [26] N. Crews, C. Wittwer, and B. Gale, "Continuous-flow thermal gradient PCR," *Biomed. Microdevices*, vol. 10, no. 2, pp. 187–95, Apr. 2008.
- [27] Y. Zhang and P. Ozdemir, "Microfluidic DNA amplification-A review," *Anal. Chim. Acta*, vol. 638, no. 2, pp. 115–125, 2009.
- [28] C. Zhang, H. Wang, and D. Xing, "Multichannel oscillatory-flow multiplex PCR microfluidics for high-throughput and fast detection of foodborne bacterial pathogens," *Biomed. Microdevices*, vol. 13, no. 5, pp. 885–897, 2011.
- [29] J. Chiou, P. Matsudaira, A. Sonin, and D. Ehrlich, "A closed-cycle capillary polymerase chain reaction machine," *Anal. Chem.*, vol. 73, no. 9, pp. 2018–2021, 2001.
- [30] L. Chen, J. West, P. Aurox, A. Manz, and P. Day, "Ultrasensitive PCR and Real-Time Detection from Human Genomic Samples Using a Bidirectional Flow Microreactor," *Anal Chem*, vol. 79, no. 23, pp. 9185–9190, 2007.
- [31] H. Wang, C. Zhang, and D. Xing, "Simultaneous detection of *Salmonella enterica*, *Escherichia coli* O157:H7, and *Listeria monocytogenes* using oscillatory-flow multiplex PCR," *Microchim. Acta*, vol. 173, no. 3–4, pp. 503–512, 2011.
- [32] S. Furutani, N. Naruishi, Y. Hagihara, and H. Nagai, "Development of an on-site rapid real-time polymerase chain reaction system and the characterization of suitable DNA polymerases for TaqMan probe technology," *Anal. Bioanal. Chem.*, pp. 1–8, 2016.
- [33] S. Brunklaus, T. E. Hansen-Hagge, J. Erwes, J. H??th, M. Jung, D. Latta, X. Strobach, C. Winkler, M. Ritzi-Lehnert, and K. S. Drese, "Fast nucleic acid amplification for integration in point-of-care applications," *Electrophoresis*, vol. 33, no. 21, pp. 3222–3228, 2012.
- [34] A. G. Sciancalepore, A. Polini, E. Mele, S. Girardo, R. Cingolani, and D. Pisignano, "Rapid nested-PCR for tyrosinase gene detection on chip," *Biosens. Bioelectron.*, vol. 26, no. 5, pp. 2711–2715, 2011.
- [35] J.-Y. Cheng, C.-J. Hsieh, Y.-C. Chuang, and J.-R. Hsieh, "Performing microchannel temperature cycling reactions using reciprocating reagent shuttling along a radial temperature gradient," *Analyst*, vol. 130, no. 6, pp. 931–940, 2005.

- [36] N. Crews, C. T. Wittwer, J. Montgomery, R. Pryor, and B. Gale, "Spatial DNA melting analysis for genotyping and variant scanning," *Anal. Chem.*, vol. 81, no. 6, pp. 2053–8, Mar. 2009.
- [37] P. J. Obeid, T. K. Christopoulos, H. J. Crabtree, and C. J. Backhouse, "Microfabricated device for DNA and RNA amplification by continuous-flow polymerase chain reaction and reverse transcription-polymerase chain reaction with cycle number selection," *Anal. Chem.*, vol. 75, no. 2, pp. 288–95, Jan. 2003.
- [38] C.-S. Liao, G.-B. Lee, H.-S. Liu, T.-M. Hsieh, and C.-H. Luo, "Miniature RT-PCR system for diagnosis of RNA-based viruses," *Nucleic Acids Res.*, vol. 33, no. 18, p. e156, Jan. 2005.
- [39] N. M. Toriello, C. N. Liu, and R. A. Mathies, "Multichannel Reverse Transcription-Polymerase Chain Reaction Microdevice for Rapid Gene Expression and Biomarker Analysis," vol. 78, no. 23, pp. 7997–8003, 2006.
- [40] G. V Kaigala, V. N. Hoang, A. Stickel, J. Lauzon, D. Manage, L. M. Pilarski, and C. J. Backhouse, "An inexpensive and portable microchip-based platform for integrated RT-PCR and capillary electrophoresis," *Analyst*, vol. 133, no. 3, pp. 331–8, Mar. 2008.
- [41] P. J. Obeid and T. K. Christopoulos, "Continuous-flow DNA and RNA amplification chip combined with laser-induced fluorescence detection," *Anal. Chim. Acta*, vol. 494, no. 1–2, pp. 1–9, Oct. 2003.
- [42] Y. Li, C. Zhang, and D. Xing, "Integrated microfluidic reverse transcription-polymerase chain reaction for rapid detection of food- or waterborne pathogenic rotavirus," *Anal. Biochem.*, vol. 415, no. 2, pp. 87–96, Aug. 2011.
- [43] K. Yamanaka, M. Saito, K. Kondoh, M. M. Hossain, R. Koketsu, T. Sasaki, N. Nagatani, K. Ikuta, and E. Tamiya, "Rapid detection for primary screening of influenza A virus: microfluidic RT-PCR chip and electrochemical DNA sensor," *Analyst*, vol. 136, no. 10, pp. 2064–8, May 2011.
- [44] D. C. Saunders, G. L. Holst, C. R. Phaneuf, N. Pak, M. Marchese, N. Sondej, M. McKinnon, and C. R. Forest, "Rapid, quantitative, reverse transcription PCR in a polymer microfluidic chip," *Biosens. Bioelectron.*, vol. 44, pp. 222–8, Jun. 2013.
- [45] I. Pješčić, C. Tranter, P. L. Hindmarsh, and N. D. Crews, "Glass-composite prototyping for flow PCR with in situ DNA analysis," *Biomed. Microdevices*, vol. 12, no. 2, pp. 333–343, 2010.
- [46] J.-W. Choi, S. Kim, R. Trichur, H. J. Cho, A. Puntambekar, R. L. Cole, J. R. Simkins, S. Murugesan, K. Kim, J.-B. J. B. Lee, G. Beaucage, J. H. Nevin, and C. H. Ahn, "A Plastic Micro Injection Molding Technique Using Replaceable Mold-Disks for Disposable Microfluidic Systems and Biochips," in *Micro Total Analysis Systems 2001: Proceedings of the micro-TAS 2001 Symposium, held in Monterey*,

CA, USA 21--25 October, 2001, J. M. Ramsey and A. van den Berg, Eds. Dordrecht: Springer Netherlands, 2001, pp. 411–412.

- [47] C. H. Ahn, J. W. Choi, G. Beaucage, J. H. Nevin, J. B. Lee, A. Puntambekar, and J. Y. Lee, “Disposable smart lab on a chip for point-of-care clinical diagnostics,” *Proc. IEEE*, vol. 92, no. 1, pp. 154–173, 2004.
- [48] C. W. Tsao and D. L. DeVoe, “Bonding of thermoplastic polymer microfluidics,” *Microfluid. Nanofluidics*, vol. 6, no. 1, pp. 1–16, 2009.
- [49] J. D. Pegan, A. Y. Ho, M. Bachman, and M. Khine, “Flexible shrink-induced high surface area electrodes for electrochemiluminescent sensing,” *Lab Chip*, vol. 13, no. 21, pp. 4205–9, 2013.
- [50] Z. J. Jia, Q. Fang, and Z. L. Fang, “Bonding of glass microfluidic chips at room temperatures,” *Anal. Chem.*, vol. 76, no. 18, pp. 5597–5602, 2004.
- [51] L. Chen, G. Luo, K. Liu, J. Ma, B. Yao, Y. Yan, and Y. Wang, “Bonding of glass-based microfluidic chips at low- or room-temperature in routine laboratory,” *Sensors Actuators, B Chem.*, vol. 119, no. 1, pp. 335–344, 2006.
- [52] Y. Xu, C. Wang, Y. Dong, L. Li, K. Jang, K. Mawatari, T. Suga, and T. Kitamori, “Low-temperature direct bonding of glass nanofluidic chips using a two-step plasma surface activation process,” *Anal. Bioanal. Chem.*, vol. 402, no. 3, pp. 1011–1018, 2012.
- [53] M. M. R. Howlader, S. Suehara, and T. Suga, “Room temperature wafer level glass/glass bonding,” *Sensors Actuators, A Phys.*, vol. 127, no. 1, pp. 31–36, 2006.
- [54] I. Pjescic and N. Crews, “Genotyping from saliva with a one-step microdevice,” *Lab Chip*, vol. 12, no. 14, pp. 2514–2519, 2012.
- [55] V. Baier, R. Födisch, A. Ihring, E. Kessler, J. Lerchner, G. Wolf, J. M. Köhler, M. Nietzsche, and M. Krügel, “Highly sensitive thermopile heat power sensor for micro-fluid calorimetry of biochemical processes,” *Sensors Actuators A Phys.*, vol. 123–124, pp. 354–359, Sep. 2005.
- [56] J. Lerchner, A. Wolf, G. Wolf, V. Baier, E. Kessler, M. Nietzsche, and M. Krügel, “A new micro-fluid chip calorimeter for biochemical applications,” *Thermochim. Acta*, vol. 445, no. 2, pp. 144–150, Jun. 2006.
- [57] J. Lerchner, A. Wolf, F. Buchholz, F. Mertens, T. R. Neu, H. Harms, and T. Maskow, “Miniaturized calorimetry — A new method for real-time biofilm activity analysis,” *J. Microbiol. Methods*, vol. 74, no. 2–3, pp. 74–81, 2008.
- [58] L. M. Ahmad, B. Towe, A. Wolf, F. Mertens, and J. Lerchner, “Binding event measurement using a chip calorimeter coupled to magnetic beads,” *Sensors Actuators B Chem.*, vol. 145, no. 1, pp. 239–245, Mar. 2010.



- [59] S. M. Tangutooru, V. L. Koppaathy, G. G. Nestorova, and E. J. Guilbeau, "Dynamic thermoelectric glucose sensing with layer-by-layer glucose oxidase immobilization," *Sensors Actuators B Chem.*, vol. 166–167, no. 0, pp. 637–641, May 2012.
- [60] V. L. Koppaathy, S. M. Tangutooru, and E. J. Guilbeau, "Label Free Detection of L-Glutamate Using Microfluidic Based Thermal Biosensor," *Bioengineering*, vol. 2, no. 1, pp. 2–14, 2015.
- [61] G. G. Nestorova and E. J. Guilbeau, "Thermoelectric method for sequencing DNA," *Lab Chip*, vol. 11, no. 10, pp. 1761–1769, 2011.
- [62] S.-I. Yoon, S.-C. Park, and Y.-J. Kim, "A micromachined microcalorimeter with split-flow microchannel for biochemical sensing applications," *Sensors Actuators B Chem.*, vol. 134, no. 1, pp. 158–165, 2008.
- [63] B. S. Kwak, B. S. Kim, H. H. Cho, J. S. Park, and H. I. Jung, "Dual thermopile integrated microfluidic calorimeter for biochemical thermodynamics," *Microfluid. Nanofluidics*, vol. 5, no. 2, pp. 255–262, 2008.
- [64] V. L. Koppaathy, S. M. Tangutooru, G. G. Nestorova, and E. J. Guilbeau, "Thermoelectric microfluidic sensor for bio-chemical applications," *Sensors Actuators B Chem.*, vol. 166–167, no. 0, pp. 608–615, May 2012.
- [65] G. G. Nestorova, V. L. Koppaathy, N. D. Crews, and E. J. Guilbeau, "Thermoelectric lab-on-a-chip ELISA," *Anal. Methods*, vol. 7, no. 5, pp. 2055–2063, 2015.